Phase Synchronization Control of Robotic Networks on Periodic Ellipses with Adaptive Network Topologies

Soon-Jo Chung* and Insu Chang †
University of Illinois at Urbana-Champaign, Urbana, IL, 61801, USA
Fred Y. Hadaegh‡
Jet Propulsion Laboratory, California Institute of Technology, Pasadena, CA, 91109, USA

This paper presents a novel formation control method for a large number of robots or vehicles described by Euler-Lagrange (EL) systems moving in elliptical orbits. A new coordinate transformation method for phase synchronization of networked EL systems in elliptical trajectories is introduced to define desired formation patterns. The proposed phase synchronization controller synchronizes the motions of agents, thereby yielding a smaller synchronization error than an uncoupled control law in the presence of bounded disturbances. A complex time-varying and switching network topology, constructed by the adaptive graph Laplacian matrix, relaxes the standard requirement of consensus stability, even permitting stabilization on an arbitrary unbalanced graph. The proofs of stability are constructed by robust contraction analysis, a relatively new nonlinear stability tool. An example of reconfiguring swarms of spacecraft in Low Earth Orbit shows the effectiveness of the proposed phase synchronization controller for a large number of complex EL systems moving in elliptical orbits.

I. Introduction

Cooperative control in robotic networks has been receiving considerable attention due to its numerous applications ranging from underwater[29] and ground vehicles to spacecraft formation flying.[2,26] More challenging applications of cooperative control include a new formation flying mission to fly swarms of spacecraft.[8,17] The sheer number of spacecraft involved in spacecraft swarms significantly complicates the formation control problem.

The objective of this paper is to introduce a new control strategy that can reduce the complexity of controlling thousands of EL systems moving in multiple elliptical orbits. This problem is motivated by elliptical relative motions of multiple spacecraft in Earth's gravitational field. However, the elliptical trajectories are also used for guidance problems in unmanned aerial vehicles[20] and obstacle avoidance of multiple autonomous underwater vehicles.[7]

There have been a variety of studies on cooperative control/estimation in networked systems. Olfati-Saber & Murray[19] investigated the average consensus problem for directed graphs with time delays. Fax & Murray[6] considered a decentralized control law for networked vehicles, constructed by identical linear time-invariant (LTI) systems. Cortés et al.[4] presented a coverage control method based on a gradient descent algorithm. A path following synchronization controller that exploits passivity properties was proposed by Ihle et al.[12] Nešić & Teel[18] derived a global asymptotic stability condition for networked systems by using input-to-state stability (ISS). Rüffer et al.[25] identified connections between cooperative systems and ISS for large-scale systems by means of a comparison principle.[13] Hong, Hu & Gao[10] and Hong, Chen & Bushnell[9] proposed a leader-follower tracking controller on a time-varying network topology. However, the stability of discontinuous intervals of the variable topology was not analyzed. Smith & Hadaegh[28] investigated stability

*Assistant Professor, Department of Aerospace Engineering, sjchung@illinois.edu, AIAA Senior Member
†Graduate Research Assistant, Department of Aerospace Engineering, chang162@illinois.edu
‡JPL Fellow and Senior Research Scientist, Guidance and Control Analysis Group, fred.y.hadaegh@jpl.nasa.gov, AIAA Fellow

conditions of a decentralized estimator, while Subbotin & Smith[30] studied a more generalized state estimator for distributed LTI systems via convex optimization. Ren & Beard[24] solved consensus problems with a time-varying topology and directed graphs. However, most prior work used simplified dynamic models (e.g., LTI systems or double integrator dynamics) in contrast with EL systems considered in this paper. Many networked dynamic systems are more accurately modeled as highly nonlinear systems, which often necessitate sophisticated nonlinear control methods along with rigorous nonlinear stability proofs. Most prior studies dealing with switching topologies focused on the stability problem itself but did not suggest how to change the network topology.

The tracking control problem can be formulated either as a leader-follower problem or a leaderless case.[23] However, a leaderless formation control might result in unwanted formation drifts. We can expect smaller state errors if tracking control is considered together with the synchronization, which is one of the contributions of this paper. For periodic motion control, a cyclic pursuit strategy for cooperative control of multi-agents in three-dimensional (3D) space was investigated by Kim & Sugie[14] where circular motions were considered. Chung & Slotine[3] presented a generalization of the average consensus problem of networked EL systems possibly with a smooth time-varying topology by combining the tracking and synchronization problems. Another contribution of[3] is to construct a very complex stabilizing network by using concurrent synchronization. Based on,[3] a combined controller for attitude and trajectory motions of spacecraft formation flying was introduced in,[2] which utilizes phase synchronization in circular motions.

In this paper, we present the phase synchronization control of multiple EL systems whose translational state variables follow multiple elliptical orbits. The synchronization in this paper means exact matching of all variables rotated by prescribed phase angles. We summarize the main contributions of the paper as follows.

First, the proposed phase synchronization controller automatically generates a time-varying network topology by means of the adaptive graph Laplacians and the distance-based connectivity method whose preliminary results were presented in.[1] Note that the connectivity method determines the number of communicating neighbors so that a computational burden can be reduced accordingly. This way, a large number of agents in a network can be effectively synchronized and reconfigured without having to define stabilizing network topologies a priori. The phase synchronization controller eliminates the need for having a balanced graph (i.e., the number of inputs from neighboring agents equals the number of outputs) for synchronization.[19]

Second, we prove exponential stability for the highly complicated and networked EL systems controlled by the proposed formation controller in the presence of disturbances and model uncertainties. The proposed controller ensures a smaller synchronization error in the presence of model uncertainties than an uncoupled tracking controller. This justifies the combined synchronization and tracking control framework for robotic networks, first introduced in.[3] For the nonlinear stability proofs, we use contraction analysis,[16] which has recently been successfully applied to network systems.[3, 21, 31]

Third, the proposed coordinate transformation method and the phase angle shift method facilitate a phase angle shift in any ellipse in 3D space so that the elliptical motions of the networked EL system can be described by the combination of *circular* and *sinusoidal* motions in a new coordinate system. We investigate the effectiveness of the proposed methods by simulating swarms of spacecraft rotating and reconfiguring in multiple periodic relative orbits. The phase difference between agents on a periodic orbit implies collision-free motions. In addition, we show how to generate collision-free maneuvers when we reconfigure a networked EL system from one orbit to another orbit.

The paper is organized as follows: In Section II, the problem statement is given with a motivating example of controlling swarms of spacecraft. The phase angle shift method for periodic elliptical orbits are introduced in Section III. The proposed phase synchronization control law is given in Section IV while stability proofs are given in Section V. In Section VI, results of simulation are discussed. Concluding remarks are given in Section VII.

II. Problem Statement and Preliminaries

In this paper, $s_{(\cdot)} = \sin(\cdot)$ and $c_{(\cdot)} = \cos(\cdot)$ are used. Also, $\|\cdot\|$ denotes the 2-norm, i.e., $\|\mathbf{x}\| = \sqrt{\mathbf{x}^T\mathbf{x}}$, while $\lambda_{\min}(\cdot)$ and $\lambda_{\max}(\cdot)$ denote the minimum and maximum eigenvalues. Two vectors concatenated vertically are written as $[\mathbf{q}_1; \mathbf{q}_2] = [\mathbf{q}_1^T, \mathbf{q}_2^T]^T$. A block diagonal matrix of square matrices can be expressed via the direct sum $\oplus$ such that $\mathbf{A} \oplus \mathbf{B} = \mathrm{diag}(\mathbf{A}, \mathbf{B})$. A block diagonal matrix of a series of p matrices can be

written as $[\mathbf{A}] = \mathbf{A}_1 \oplus \mathbf{A}_2 \oplus \cdots \oplus \mathbf{A}_p$) while the brackets $\{\mathbf{q}\}$ are reserved for a concatenated vector. Also, $\mathbf{A} \otimes \mathbf{B} \in \mathbb{R}^{mp \times nq}$ denotes the Kronecker product of $\mathbf{A} \in \mathbb{R}^{m \times n}$ and $\mathbf{B} \in \mathbb{R}^{p \times q}$. Also, $\mathbf{I}_n \in \mathbb{R}^{n \times n}$ denotes an identify matrix.

For a robotic network consisting of p EL systems, the dynamic model of the jth agent ($1 \leq j \leq p$) is given as

$$\mathbf{M}_j(\mathbf{q}_j)\ddot{\mathbf{q}}_j + \mathbf{C}_j(\mathbf{q}_j, \dot{\mathbf{q}}_j)\dot{\mathbf{q}}_j + \mathbf{G}_j(\mathbf{q}_j) = \boldsymbol{\tau}_j - \mathbf{D}_j(\mathbf{q}_j, \dot{\mathbf{q}}_j) \tag{1}$$

where $\mathbf{q}_j \in \mathbb{R}^n$ denotes a vector of configuration variables that can encompass both translational ($\mathbf{q}_{j,\text{tr}} \in \mathbb{R}^3$)and rotational (e.g. robot joint or attitude) motions denoted by $\mathbf{q}_{j,\text{other}} \in \mathbb{R}^{n-3}$ such that

$$\mathbf{q}_j = [\mathbf{q}_{j,\text{other}}; \mathbf{q}_{j,\text{tr}}] \tag{2}$$

where $\mathbf{q}_{j,\text{other}} = [q_{j,1}, \cdots, q_{j,n-3}]^T$, $\mathbf{q}_{j,\text{tr}} = [x_j, y_j, z_j]^T$. One example is a rigid body motion on SE(3). The inertia matrix $\mathbf{M}_j(\mathbf{q}_j) > 0$ is assumed to be upper bounded and can be written as $\mathbf{M}_j(\mathbf{q}_j) = \mathbf{M}_{j,\text{other}}(\mathbf{q}_{j,\text{other}}) \oplus m_j\mathbf{I}_3$. Also, $\mathbf{M}_j(\mathbf{q}_j) \in \mathbb{R}^{n \times n}$, $\mathbf{C}_j(\mathbf{q}_j, \dot{\mathbf{q}}_j) \in \mathbb{R}^{n \times n}$, $\mathbf{G}_j(\mathbf{q}_j) \in \mathbb{R}^n$, $\boldsymbol{\tau}_j \in \mathbb{R}^n$, and $\mathbf{D}_j \in \mathbb{R}^n$ denote the inertia matrix, the Coriolis/centrifugal forces, the gravitational force, the control input, and the non-conservative forces, respectively. Note that $\mathbf{C}_j(\mathbf{q}_j, \dot{\mathbf{q}}_j)$ is chosen such that $\dot{\mathbf{M}}_j(\mathbf{q}_j) - 2\mathbf{C}_j(\mathbf{q}_j, \dot{\mathbf{q}}_j)$ is skew-symmetric. This property is essential to our stability proofs.

We want to design a tracking and phase synchronization control law such that each EL system in the network can yield a bounded error with respect to its desired trajectory and the trajectories of its neighbors. The translation motions of the networked EL systems may follow multiple concentric ellipses as shown in Fig. 1. We use a single or multiple leader agents to define and reconfigure the desired trajectories as needed.

Controlling swarms of spacecraft in Low Earth Orbit (LEO) is our motivating example for the present

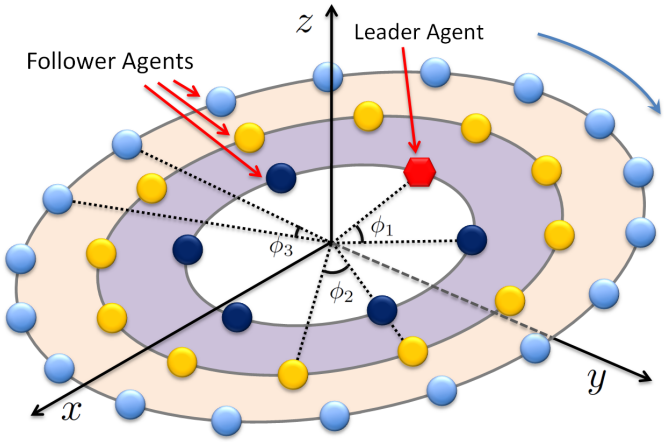

Figure 1. Problem formulation: multiple EL systems on concentric elliptical orbits in 3D space with phase angle differences.

paper.

Example 1 [17] *The relative translational motion of each spacecraft in the swarm is written with respect to the Local Vertical Local Horizontal (LVLH) frame. The origin of the LVLH frame, called the chief orbital motion, is described by the classical orbital elements* ($\mathbf{oe}$)[a] *defined in the Earth Centered Inertial (ECI) frame (see Fig. 2). Note that Fig. 1 shows that the chief motion differs from the leader agent. The relative translational motion,* $\mathbf{q}_j = [x_j,\ y_j,\ z_j]^T$ *of the* j*th spacecraft in the presence of Earth's oblateness (*J_2 *effect) and atmospheric drag can be written in the form of (1) with* $(\dot{\mathbf{M}}_j - 2\mathbf{C}_j)$ *being still skew-symmetric despite*

[a] $\mathbf{oe} := [a,\ e,\ i,\ \Omega,\ \omega,\ \nu]$, where a, e, i, Ω, ω, ν denote the semimajor axis, eccentricity, inclination, right ascension of ascending node, argument of perigee, and true anomaly.

$\dot{\mathbf{M}}_j = \mathbf{0}$.

$$
\begin{aligned}
&\mathbf{M}_j\ddot{\mathbf{q}}_j + \mathbf{C}_j(t)\dot{\mathbf{q}}_j + \mathbf{G}_j(\mathbf{q}_j, \boldsymbol{\varpi}(t)) + \mathbf{D}_j(\mathbf{q}_j, \dot{\mathbf{q}}_j, \boldsymbol{\varpi}(t)) = \boldsymbol{\tau}_j \\
&\mathbf{M}_j = m_j\mathbf{I}_3,\ \mathbf{C}_j(\boldsymbol{\varpi}(t)) = 2m_j \begin{bmatrix} 0 & -\omega_z & 0 \\ \omega_z & 0 & -\omega_x \\ 0 & \omega_x & 0 \end{bmatrix}, \\
&\mathbf{G}_j = m_j \begin{bmatrix} x_j(\eta_j^2-\omega_z^2) - y_j\alpha_z + z_j\omega_x\omega_z + (\zeta_j-\zeta)s_i s_\theta + r(\eta_j^2-\eta^2) \\ x_j\alpha_z + y_j(\eta_j^2-\omega_z^2-\omega_x^2) - z_j\alpha_x + (\zeta_j-\zeta)s_i c_\theta \\ x_j\omega_x\omega_z + y_j\alpha_x + z_j(\eta_j^2-\omega_x^2) + (\zeta_j-\zeta)c_i \end{bmatrix} \\
&\mathbf{D}_j = \begin{bmatrix} -\dot{x}_j D_j v_{j\mathrm{r}} + y_j D_j v_{j\mathrm{r}}\omega_z - (D_j v_{j\mathrm{r}} - D v_\mathrm{r}) R_1 \mathbf{V}_\mathrm{r} \\ -\dot{y}_j D_j v_{j\mathrm{r}} - x_j D_j v_{j\mathrm{r}}\omega_z + z_j D_j v_{j\mathrm{r}}\omega_x - (D_j v_{j\mathrm{r}} - D v_\mathrm{r}) R_2 \mathbf{V}_\mathrm{r} \\ -\dot{z}_j D_j v_{j\mathrm{r}} - y_j D_j v_{j\mathrm{r}}\omega_x - (D_j v_{j\mathrm{r}} - D v_\mathrm{r}) R_3 \mathbf{V}_\mathrm{r} \end{bmatrix}
\end{aligned}
\tag{3}
$$

where θ, m_j, $\mathbf{G}_j(\mathbf{q}_j, \boldsymbol{\varpi}(t))$, and $\mathbf{D}_j(\mathbf{q}_j, \dot{\mathbf{q}}_j, \boldsymbol{\varpi}(t))$ denote the argument of latitude, the mass, the gravitational force, and atmospheric drag of the jth spacecraft, respectively. The angular acceleration in the LVLH frame is $\dot{\boldsymbol{\omega}}_\mathrm{I} = [\alpha_x,\ \alpha_y,\ \alpha_z]^T = [\dot{\omega}_x,\ \dot{\omega}_y,\ \dot{\omega}_z]^T$. The symbols used here are defined as follows[17] : $\kappa = \sqrt{1-e^2}$, $\chi = 1 + ec_\nu$, $\eta^2 = \frac{\mu}{r^3} + \frac{k_{J_2}}{r^5} - \frac{5k_{J_2}s_i^2 s_\theta^2}{r^5}$, $\eta_j^2 = \frac{\mu}{r_j^3} + \frac{k_{J_2}}{r_j^5} - \frac{5k_{J_2}r_{jZ}^2}{r_j^7}$, $\zeta = \frac{2k_{J_2}s_i s_\theta}{r^4}$, $\zeta_j = \frac{2k_{J_2}r_{jZ}}{r_j^5}$, $\omega_x = -\frac{k_{J_2}s_{2i}s_\theta}{hr^3} - \frac{\kappa D v_\mathrm{r} R_3 \mathbf{V}_\mathrm{r}}{na\chi}$, $\omega_y = 0$, $\omega_z = \frac{n\chi^2}{\kappa^3}$, $h = na^2\kappa$, and $r_{jZ} = (r + x_j)s_i s_\theta + y_j s_i c_\theta + z_j c_i$. Also, $D_j = \frac{1}{2}C_{Dj}A_j\rho_j$, where C_{Dj} is a drag coefficient, A_j the cross-sectional area, and ρ_j the air density for the jth spacecraft. The magnitude of the velocity is denoted by $v_{j\mathrm{r}}$. The symbols without the subscript j indicate the values for the chief orbital motion.

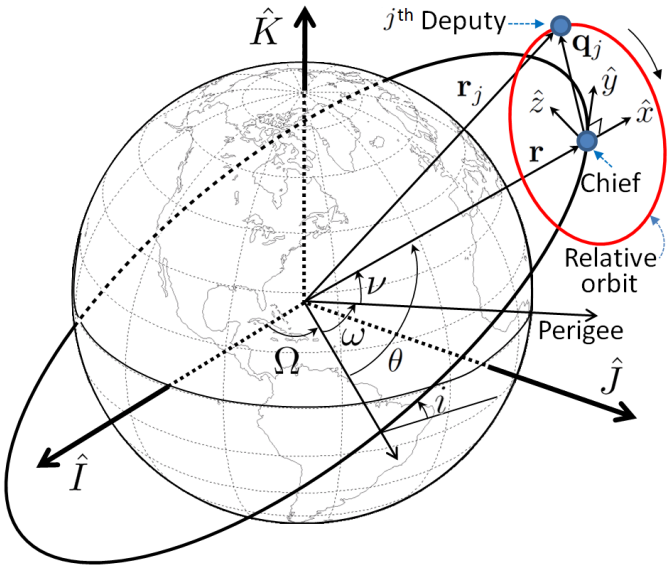

Figure 2. ECI ($\hat{I}$, $\hat{J}$, $\hat{K}$) and LVLH ($\hat{x}$, $\hat{y}$, $\hat{z}$) frames.

In this paper, the agents are assumed to move in elliptical (relative) orbits. We assume that there is an out-of-plane motion to form an ellipse in 3D space such that

$$
x_d(t) = x_e s_{(\psi+\psi_{e_0})},\ y_d(t) = y_e c_{(\psi+\psi_{e_0})},\ z_d(t) = z_e s_{(\psi+\psi_{z_0})} \tag{4}
$$

where x_e, y_e, z_e are the amplitudes. The angular rate n is defined such that $\dot{\psi} = n$. Also, ψ_{e_0} and ψ_{z_0} are initial conditions for ψ_e and ψ_z.

Example 2 *(3) can be linearized in the absence of all the perturbation terms, resulting in a linear differential equation called the Hill-Clohessy-Wiltshire (HCW) equation. The solution to this linear HCW equation can then easily be obtained. Furthermore, if the initial conditions satisfy $\dot{y}_0 = -2nx_0$ and $\dot{x}_0 = ny_0/2$, the solutions of the HCW equations result in a periodic elliptical motion:*

$$
x_d(t) = a_e s_{\psi_e},\ y_d(t) = 2a_e c_{\psi_e},\ z_d(t) = z_{\max} s_{\psi_z} \tag{5}
$$

where $n = \sqrt{\mu/a^3}$, $a_e = \sqrt{(\dot{x}_0/n)^2 + (3x_0 + 2\dot{y}_0/n)^2}$, $\psi_e = \psi - \psi_{e_0}$, $\psi = nt$, $\psi_{e_0} = \tan^{-1}\left((3nx_0 + 2\dot{y}_0)/\dot{x}_0\right)$, $z_{\max} = \sqrt{z_0^2 + (\dot{z}_0/n)^2}$, $\psi_z = \psi + \psi_{z_0}$, *and* $\psi_{z_0} = \tan^{-1}\left(nz_0/\dot{z}_0\right)$. *Note that the solutions describe elliptical orbits with the relative semimajor axis* $(2a_e)$ *and the relative semiminor axis* (a_e) *in the* x*-*y *plane.*

For additional initial conditions to obtain J_2-invariant relative orbits, readers are referred to[17] for details.

III. Phase Angle Shift in Elliptical Orbits

A. Derivation of New Coordinate Transformation

The time-varying vector $\mathbf{q}_d(t)$ denotes the desired trajectory or the trajectory of a leader agent. In this section, we derive a desired position vector $\mathbf{q}_{d,j,\mathrm{tr}} = [x_{d,j}, y_{d,j}, z_{d,j}]^T$ from a single pre-determined desired trajectory $\mathbf{q}_{d,\mathrm{tr}}$, shown in (4), or a leader agent moving in an elliptical orbit (see Fig. 1). We assume that the leader trajectory can be relayed between the agents. Performing a phase angle shift on an ellipse is not straightforward. As shown in Fig. 1, a constant angular rate $n = \dot{\psi}$ results in a time-varying phase difference angle ϕ on each ellipse. The following lemma can be used to perform an angle shift with a constant ϕ on an elliptical orbit.

Lemma 1 *For a networked EL system moving in an elliptical orbit (4), there exists a coordinate transformation matrix such that* $\mathbf{q}'_d = \mathbf{R}_{\mathrm{f}}\mathbf{q}_d$, *where the original elliptical orbit of* $\mathbf{q}_{d,\mathrm{tr}} = [x_d, y_d, z_d]^T$ *is mapped into a combination of a circular motion in the* x'*-*y' *plane and a sinusoidal function in the* z' *axis, where* $\mathbf{q}'_{d,\mathrm{tr}} = [x'_d, y'_d, z'_d]^T$.

Proof: We consider two consecutive coordinate transformations. First, we transform the original frame to the intermediate frame whose x^N-y^N plane encompasses the elliptical orbit (see Fig. 3). The distance between the origin and the agent can be found from (4) as

$$l(\psi) = \sqrt{x_e^2 s^2_{(\psi+\psi_{e_0})} + y_e^2 c^2_{(\psi+\psi_{e_0})} + z_e^2 s^2_{(\psi+\psi_{z_0})}} \tag{6}$$

Hence, $l(\psi)$ has the following extrema: $l_{\min} = l(-\Phi)$ and $l_{\max} = l(3\pi/2 - \Phi)$ since

$$\begin{aligned} \frac{dl}{d\psi} &= \frac{s_{(2\psi+2\Phi)}\sqrt{(x_e^2 - y_e^2 + z_e^2)^2 - 4(x_e^2 - y_e^2)z_e^2 s^2_{(\psi_{e_0}-\psi_{z_0})}}}{2l} \\ \Phi &= \tfrac{1}{2}\tan^{-1}\left(\frac{(x_e^2 - y_e^2)s_{(2\psi_{e_0})} + z_e^2 s_{(2\psi_{z_0})}}{(x_e^2 - y_e^2)c_{(2\psi_{e_0})} + z_e^2 c_{(2\psi_{z_0})}}\right) \end{aligned} \tag{7}$$

The unit vectors for the positions of $l_{\min}$ and $l_{\max}$ in the original frame are defined as $\hat{x}^N$ and $\hat{y}^N$ for the intermediate frame. The last axis $\hat{z}^N$ is obtained by $\hat{z}^N = \hat{x}^N \times \hat{y}^N$. If $\{\hat{x},\ \hat{y},\ \hat{z}\}$ are defined as the orthonormal unit vectors for the original frame, then the first rotational transformation matrix $\mathbf{R}_{\mathrm{nf}} \in \mathbb{R}^{n\times n}$ is obtained by using a direction cosine matrix such that

$$\mathbf{R}'_{\mathrm{nf}} = \begin{bmatrix} -\frac{x_e}{l_{\min}} s_{(\Phi-\psi_{e_0})} & \frac{y_e}{l_{\min}} c_{(\Phi-\psi_{e_0})} & -\frac{z_e}{l_{\min}} s_{(\Phi-\psi_{z_0})} \\ -\frac{x_e}{l_{\max}} c_{(\Phi-\psi_{e_0})} & -\frac{y_e}{l_{\max}} s_{(\Phi-\psi_{e_0})} & -\frac{z_e}{l_{\max}} c_{(\Phi-\psi_{z_0})} \\ -\frac{y_e z_e}{l_{\min} l_{\max}} c_{(\psi_{e_0}-\psi_{z_0})} & \frac{x_e z_e}{l_{\min} l_{\max}} s_{(\psi_{e_0}-\psi_{z_0})} & \frac{x_e y_e}{l_{\min} l_{\max}} \end{bmatrix}.$$

$$\text{and } \mathbf{R}_{\mathrm{nf}} = \mathbf{I}_{n-3} \oplus \mathbf{R}'_{\mathrm{nf}} \tag{8}$$

where we can verify $\mathbf{R}'_{\mathrm{nf}}{\mathbf{R}'_{\mathrm{nf}}}^T = {\mathbf{R}'_{\mathrm{nf}}}^T\mathbf{R}'_{\mathrm{nf}} = \mathbf{I}_3$. The second rotation is related to finding an angle (ψ_x) with respect to the x^N axis such that the motion in the new x'-y' plane becomes *circular*. We can notice from Fig. 3 that $l_{\min}$ becomes a radius of the circle in the new frame. Therefore, $\psi_x \geq 0$ can be expressed as[b]

$$\psi_x = \cos^{-1}\left(l_{\min}/l_{\max}\right) \tag{9}$$

Figure 3 illustrates the definition of ψ_x and the geometrical relationship between the two frames.
The second transformation matrix $\mathbf{R}_{\mathrm{ns}} \in \mathbb{R}^{n\times n}$ is defined as

$$\mathbf{R}_{\mathrm{ns}}(\psi_x) = \mathbf{I}_{n-3} \oplus \mathbf{R}'_{\mathrm{ns}}(\psi_x) = \mathbf{I}_{n-3} \oplus \begin{bmatrix} 1 & 0 & 0 \\ 0 & c_{\psi_x} & s_{\psi_x} \\ 0 & -s_{\psi_x} & c_{\psi_x} \end{bmatrix} \tag{10}$$

[b]From Fig. 3, ψ_x has dual values with different signs in $[-\pi/2,\ \pi/2]$. We define ψ_x as a non-negative angle.

Hence, the coordinate transformation from the original frame to the new frame can be found by (8) and (10):

$$\mathbf{q}'_d(t) = \Big(\mathbf{R}_{\rm ns}(\psi_x)\mathbf{R}_{\rm nf}\Big)\mathbf{q}_d =: \mathbf{R}_{\rm f}\mathbf{q}_d(t) \in \mathbb{R}^n \tag{11}$$

where $\mathbf{q}'_d = [q_{d,1},\ q_{d,2},\ \cdots,\ q_{d,(n-3)},\ x'_d,\ y'_d,\ z'_d]^T$. ■

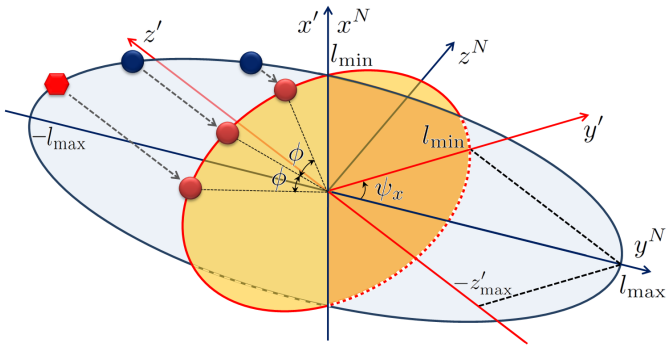

Figure 3. The angular rotation ψ_x transforms the intermediate frame (x^N-y^N-z^N) to the new frame (x'-y'-z').

Now we are ready to show how to shift the position of each member with only one phase shift angle ϕ.

Lemma 2 *Given the new coordinate system by $\mathbf{R}_{\rm f}$ in (11), there exists a phase angle shift matrix $\mathbf{T}((j-1)\phi) \in \mathbb{R}^{(n+1)\times(n+1)}$ such that the jth agent can shift its position by $(j-1)\phi$ from the leader agent.*

Proof: From the definition of an ellipse in (4), the phase angle shift for the x'-y' plane is given as

$$\begin{aligned}\begin{bmatrix} x'_{d,j} \\ y'_{d,j} \end{bmatrix} &= \begin{bmatrix} c_{(j-1)\phi} & -s_{(j-1)\phi} \\ s_{(j-1)\phi} & c_{(j-1)\phi} \end{bmatrix} \begin{bmatrix} l_{\min} c_{(\psi+\Phi)} \\ -l_{\min} s_{(\psi+\Phi)} \end{bmatrix} \\ &= \mathbf{T}_z((j-1)\phi) \begin{bmatrix} x'_d \\ y'_d \end{bmatrix} \end{aligned} \tag{12}$$

For the phase angle shift in the z' axis, we define an auxiliary variable Z'_d as $Z'_d := z'_{\max} c_{(\psi+\Phi)}$ where $z'_{\max} = \sqrt{l^2_{\max} - l^2_{\min}} \geq 0$. Then the angle rotation for z'_d and Z'_d can be defined as

$$\begin{aligned}\begin{bmatrix} z'_{d,j} \\ Z'_{d,j} \end{bmatrix} &= \begin{bmatrix} c_{(j-1)\phi} & -s_{(j-1)\phi} \\ s_{(j-1)\phi} & c_{(j-1)\phi} \end{bmatrix} \begin{bmatrix} z'_{\max} s_{(\psi+\Phi)} \\ z'_{\max} c_{(\psi+\Phi)} \end{bmatrix} \\ &= \mathbf{T}_z((j-1)\phi) \begin{bmatrix} z'_d \\ Z'_d \end{bmatrix} \end{aligned} \tag{13}$$

Hence, by combining (12) and (13), the proposed phase angle shift for the jth agent is given as

$$\begin{aligned} \mathbf{q}''_{d,j} &= \mathbf{T}_{j-1}\mathbf{q}''_d = \left(\mathbf{I}_{n-3} \oplus \mathbf{T}'_{j-1}\right)\mathbf{q}''_d \in \mathbb{R}^{n+1} \\ \mathbf{q}''_d &= [\mathbf{q}'_d; Z'_d] = [\mathbf{R}_{\rm f}\mathbf{q}_d; Z'_d] \end{aligned} \tag{14}$$

where $\mathbf{T}'_{j-1} = \mathbf{T}_z((j-1)\phi) \oplus \mathbf{T}_z((j-1)\phi) \in \mathbb{R}^{4\times4}$. The time derivative of $\mathbf{q}''_{d,j}$ can be obtained as $\dot{\mathbf{q}}''_{d,j} = \mathbf{T}_{j-1}\dot{\mathbf{q}}''_d \in \mathbb{R}^{n+1}$ where $\dot{\mathbf{q}}''_d = [\dot{\mathbf{q}}'_d; \dot{Z}'_d]$ with $\dot{Z}'_d = -z'_d\dot{z}'_d/Z'_d$. ■

Remark 1 The auxiliary variable Z'_d in $\mathbf{q}''_d$ is used only to apply the phase angle shift to z'_d. Thus, Z'_d can be abandoned from the state vector after the rotation.

Remark 2 If we assume that agents can communicate only with one neighbor, the desired trajectory of the jth agent is replaced by that of the $(j-1)$th agent: $\mathbf{q}_d = \mathbf{q}_{j-1}$ for the jth agent. In this case, $\mathbf{T}((j-1)\phi) = \mathbf{T}(\phi)\ \forall j\ (1 \leq j \leq p)$. Therefore, each member will follow its immediate neighbor with the phase difference ϕ.

B. Modification of Configuration Variables

In this paper, the variables with a prime ($'$) are defined in the new frame that has a circular motion in the x'-y' plane while those with a double prime ($''$) has an auxiliary $(n+1)$th variable for the angular phase shift with $\mathbf{T}_{j-1}$. We introduce new modified variables needed for the main control law in three successive steps.
[Step 1] Similar to (14), $\mathbf{q}_j$ is transformed as follows

$$\mathbf{q}'_j = \mathbf{R}_{\mathrm{f}}\mathbf{q}_j, \qquad \mathbf{q}''_j = \left[\mathbf{q}'_j; Z'_j\right] = \left[\mathbf{R}_{\mathrm{f}}\mathbf{q}_j; Z'_j\right] \tag{15}$$

where $\psi + \Phi$ from (7) is used to define

$$Z'_j = z'_{\max,j} c_{(\psi+\Phi)} = R_{\mathrm{f},3}\mathbf{q}_j \cot(\psi + \Phi) \tag{16}$$

where $z'_{\max,j} = R_{\mathrm{f},3}\mathbf{q}_j / s_{(\psi+\Phi)}$ and $R_{\mathrm{f},3}$ is the n-th row vector of $\mathbf{R}_{\mathrm{f}}$.
[Step 2] The tracking control error is expressed in terms of the modified composite variable $(\mathbf{s}''_j)$[27]

$$\mathbf{s}''_j = \dot{\mathbf{q}}''_j - \mathbf{T}_{j-1}\dot{\mathbf{q}}''_d + \mathbf{\Lambda}''(\mathbf{q}''_j - \mathbf{T}_{j-1}\mathbf{q}''_d) = \dot{\mathbf{q}}''_j - \dot{\mathbf{q}}''_{j,r} \tag{17}$$

where $\mathbf{\Lambda}'' = \lambda''\mathbf{I}_{n+1} > 0$ and $\mathbf{T}_{j-1}$ is defined in (14). Note that we can compute $\dot{\mathbf{q}}'_{j,r}$ from $\dot{\mathbf{q}}''_{j,r} = [\dot{\mathbf{q}}'_{j,r}; \dot{Z}'_{j,r}]$. Also, $\mathbf{s}''_j = [\mathbf{s}''_{j,\mathrm{other}}; \mathbf{s}''_{j,\mathrm{tr}}]$ based on (2).
[Step 3] In order to properly define the synchronization between multiple agents, $\mathbf{u}'_j$ and $\mathbf{u}''_j$ are used such that

$$\mathbf{u}''_j := \mathbf{T}^T_{j-1}\mathbf{s}''_j = \begin{bmatrix} \mathbf{u}'_j \\ u'_{jZ'} \end{bmatrix} = \begin{bmatrix} \mathbf{u}'_{j,\mathrm{other}} \\ \mathbf{u}'_{j,\mathrm{tr}} \\ u'_{jZ'} \end{bmatrix} \in \mathbb{R}^{n+1} \tag{18}$$

which can be expanded as

$$\mathbf{u}''_j = \mathbf{T}^T_{j-1}\dot{\mathbf{q}}''_j - \dot{\mathbf{q}}''_d + \mathbf{\Lambda}''(\mathbf{T}^T_{j-1}\mathbf{q}''_j - \mathbf{q}''_d) \tag{19}$$

Consequently, the synchronization error between the jth and kth members can be defined independently of $\mathbf{q}''_d(t)$

$$\mathbf{u}''_j - \mathbf{u}''_k = \mathbf{T}^T_{j-1}\dot{\mathbf{q}}''_j - \mathbf{T}^T_{k-1}\dot{\mathbf{q}}''_k + \mathbf{\Lambda}''(\mathbf{T}^T_{j-1}\mathbf{q}''_j - \mathbf{T}^T_{k-1}\mathbf{q}''_k) \tag{20}$$

IV. Phase Synchronization Control

We present the main controller in this section.

A. Phase Synchronization Controller

Given the dynamic model in (1) and the desired trajectories in (4), we should transform the original frame to the new frame by using the coordinate transformation $\mathbf{R}_{\mathrm{f}}$ in (11) such that we can use the phase angle shift method $\mathbf{T}_{j-1}$ in (14). By left-multiplying (1) by $\mathbf{R}_{\mathrm{f}}$ and $\mathbf{q}_j = \mathbf{R}^T_{\mathrm{f}}\mathbf{R}_{\mathrm{f}}\mathbf{q}_j = \mathbf{R}^T_{\mathrm{f}}\mathbf{q}'_j$, the dynamic model is expressed in the new frame as

$$\begin{aligned} &\begin{bmatrix} \mathbf{R}_{\mathrm{f}}\mathbf{M}_j(\mathbf{q}_j)\mathbf{R}^T_{\mathrm{f}} & \mathbf{0}_{n\times 1} \\ \mathbf{0}_{1\times n} & (\mathbf{R}_{\mathrm{f}}\mathbf{M}_j(\mathbf{q}_j)\mathbf{R}^T_{\mathrm{f}})_{n,n} \end{bmatrix} \ddot{\mathbf{q}}''_j \\ &+ \begin{bmatrix} \mathbf{R}_{\mathrm{f}}\mathbf{C}_j(\mathbf{q}_j,\dot{\mathbf{q}}_j)\mathbf{R}^T_{\mathrm{f}} & \mathbf{0}_{n\times 1} \\ \mathbf{0}_{1\times n} & (\mathbf{R}_{\mathrm{f}}\mathbf{C}_j(\mathbf{q}_j,\dot{\mathbf{q}}_j)\mathbf{R}^T_{\mathrm{f}})_{n,n} \end{bmatrix} \dot{\mathbf{q}}''_j \\ &+ \begin{bmatrix} \mathbf{R}_{\mathrm{f}}\mathbf{G}_j(\mathbf{R}^T_{\mathrm{f}}\mathbf{q}'_j) \\ G_{jZ'} \end{bmatrix} + \begin{bmatrix} \mathbf{R}_{\mathrm{f}}\mathbf{D}_j(\mathbf{R}^T_{\mathrm{f}}\mathbf{q}'_j, \mathbf{R}^T_{\mathrm{f}}\dot{\mathbf{q}}'_j) \\ D_{jZ'} \end{bmatrix} = \begin{bmatrix} \mathbf{R}_{\mathrm{f}}\boldsymbol{\tau}_j(t) \\ \tau_{jZ'} \end{bmatrix} \end{aligned} \tag{21}$$

where $(\mathbf{R}_{\mathrm{f}}\mathbf{M}_j\mathbf{R}^T_{\mathrm{f}})_{n,n}$ and $(\mathbf{R}_{\mathrm{f}}\mathbf{C}_j\mathbf{R}^T_{\mathrm{f}})_{n,n}$ denote the (n,n) elements of $\mathbf{R}_{\mathrm{f}}\mathbf{M}_j\mathbf{R}^T_{\mathrm{f}}$ and $\mathbf{R}_{\mathrm{f}}\mathbf{C}_j\mathbf{R}^T_{\mathrm{f}}$, respectively. Similar to (16), we can find $G_{jZ'} = R_{\mathrm{f},3}\mathbf{G}_j \cot(\psi + \Phi)$ and $D_{jZ'} = R_{\mathrm{f},3}\mathbf{D}_j \cot(\psi + \Phi)$.

Note that the matrix form in (21) is used due to the replacement of $\mathbf{q}'_j \in \mathbb{R}^n$ by $\mathbf{q}''_j \in \mathbb{R}^{n+1}$.

The active parameter adaptation is adopted for the purpose of tuning the tracking and diffusive coupling gains. These adaptive coupling gains might initiate a new communication link with neighbors or end the existing communication links. We assume that all agents can obtain the desired trajectory of the orbit leader

agent by communications with neighbors in the network. The proposed adaptive formation controller for the jth member is written as

$$\begin{aligned}\begin{bmatrix} \mathbf{R}_{\mathrm{f}}\boldsymbol{\tau}_j(t) \\ \tau_{jZ'} \end{bmatrix} &= \begin{bmatrix} \mathbf{R}_{\mathrm{f}}\hat{\mathbf{M}}_j(\mathbf{q}_j)\mathbf{R}_{\mathrm{f}}^T & \mathbf{0}_{n\times 1} \\ \mathbf{0}_{1\times n} & (\mathbf{R}_{\mathrm{f}}\hat{\mathbf{M}}_j(\mathbf{q}_j)\mathbf{R}_{\mathrm{f}}^T)_{n,n} \end{bmatrix} \ddot{\mathbf{q}}''_{j,r} \\ &+ \begin{bmatrix} \mathbf{R}_{\mathrm{f}}\hat{\mathbf{C}}_j(\mathbf{q}_j,\dot{\mathbf{q}}_j)\mathbf{R}_{\mathrm{f}}^T & \mathbf{0}_{n\times 1} \\ \mathbf{0}_{1\times n} & (\mathbf{R}_{\mathrm{f}}\hat{\mathbf{C}}_j(\mathbf{q}_j,\dot{\mathbf{q}}_j)\mathbf{R}_{\mathrm{f}}^T)_{n,n} \end{bmatrix} \dot{\mathbf{q}}''_{j,r} \\ &+ \begin{bmatrix} \mathbf{R}_{\mathrm{f}}\hat{\mathbf{D}}_j(\mathbf{R}_{\mathrm{f}}^T\mathbf{q}'_j,\mathbf{R}_{\mathrm{f}}^T\dot{\mathbf{q}}'_j) \\ \hat{D}_{jZ'} \end{bmatrix} + \begin{bmatrix} \mathbf{R}_{\mathrm{f}}\mathbf{G}_j(\mathbf{R}_{\mathrm{f}}^T\mathbf{q}'_j) \\ G_{jZ'} \end{bmatrix} - \begin{bmatrix} \mathbf{0}_{(n-3)\times 1} \\ \mathbf{T}'_{j-1}\mathcal{W}_j\mathbf{c}_j \end{bmatrix} \\ &- \begin{bmatrix} k_0\mathbf{s}''_{j,\mathrm{other}} \\ k_1(t)\mathbf{s}''_{j,\mathrm{tr}} \end{bmatrix} + \begin{bmatrix} \mathbf{0}_{(n-3)\times 1} \\ k_2(t)\frac{2}{m_o}\sum_{l\in\mathcal{N}_j(t)}^{m_o}\mathbf{T}'_{j-l}\mathbf{s}''_{l,\mathrm{tr}} \end{bmatrix} + \mathbf{Q}''_j \end{aligned} \tag{22}$$

from which $\boldsymbol{\tau}_j(t)$ can be determined since $\mathbf{R}_{\mathrm{f}}$ is invertible. The adaptive coupling gain vector $\mathbf{c}_j$ is defined in Sect. C and $\mathcal{W}_j$ is a function of the distanced-based connectivity function as discussed in Sect. B. The hat operator $\hat{(\cdot)}$ denotes a function of estimated parameters to be discussed in Sect. D. The last term, $\mathbf{Q}''_j = [\mathbf{0}_{1\times(n-3)}\ \mathbf{R}'_{\mathrm{f}}\mathbf{Q}_{j,\mathrm{tr}}\ 0]^T$, is critical for collision free motions during transient maneuvers (see Sect. E).

Remark 3 The diffusive coupling term
$k_2(t)\frac{2}{m_o}\sum_{l\in\mathcal{N}_j(t)}^{m_o}\mathbf{T}'_{j-l}\mathbf{s}''_{l,\mathrm{tr}}$ along with $k_1(t)\mathbf{s}''_{j,\mathrm{tr}}$ defines the nominal graph Laplacian matrix $\mathbf{L}_{\mathrm{tr}}$ for the constant or time-varying set $\mathcal{N}_j(t)$. One condition is that the number of neighbors ($= m_o$) is the same for each robot (i.e., regular graph). Since this nominal graph structure is augmented by an adaptive graph Laplacian constructed by $\mathbf{c}_j$ that permits additional couplings with neighbors, each robot might end up coupled with a different number of neighbors. One example we use in this paper as the nominal graph structure is a bidirectional ring:

$$\frac{2}{m_o}\sum_{l\in\mathcal{N}_j(t)}^{m_o}\mathbf{T}'_{j-l}\mathbf{s}''_{l,\mathrm{tr}} = \left(\mathbf{T}'_{j-l}\mathbf{s}''_{l,\mathrm{tr}} + \mathbf{T}'_{j-m}\mathbf{s}''_{m,\mathrm{tr}}\right) \tag{23}$$

B. Distance-Based Connectivity

The coupling gains $\mathbf{c}_j$ will be varied based on the relative distance between networked EL systems. The special connectivity ϱ_{jk} between the jth and kth agents is defined as

$$\varrho_{jk}(d_{jk}) = \begin{cases} \left(1 + e^{\beta_j(d_{jk}^2 - r_{c,j}^2)}\right)^{-1}, & \text{if } d_{jk} \le d_{\mathrm{limit},j} \\ 0, & \text{otherwise} \end{cases} \tag{24}$$

where $d_{jk} := \|\mathbf{r}_j - \mathbf{r}_k\|$. The variable $r_{c,j}$ is a critical boundary and β_j determines an inclination of ϱ_{jk} at $d_{jk} = r_{c,j}$. In (24), $d_{\mathrm{limit},j}$ is a maximum distance for communications with neighbors. Therefore, if we define $\varrho_{\mathrm{limit},j} := \varrho_{jk}(d_{\mathrm{limit},j}) > 0$, then the second condition in (24) can be rewritten as

$$\varrho_{jk}(d_{jk}) = 0 \quad \text{if} \quad \varrho_{jk}(d_{jk}) < \varrho_{\mathrm{limit},j} \tag{25}$$

Note that $d_{\mathrm{limit},j}$ can be defined as $d_{\mathrm{limit},j} := k_j r_{c,j}$ with some $k_j \in \mathbb{R}_+$. The connectivity ϱ_{jk} has the following characteristics:

- $\varrho_{jk} \approx$ constant< 1 with $d_{jk} < r_{c,j}$ and slowly decreases as d_{jk} approaches $r_{c,j}$ from $d_{jk} = 0$.
- $\varrho_{jk} = 0.5$ at $d_{jk} = r_{c,j}$.
- ϱ_{jk} decreases fast near $d_{jk} = r_{c,j}$ depending on β_j and decreases gradually as d_{jk} ($> r_{c,j}$) increases.

Remark 4 This connectivity affects the number of communications for each network in the network by changing β_j and $r_{c,j}$ in (24). Further, we can choose to impose a hard constraint on the number of communicating neighbors by setting the rest of ϱ_{jk} to zero once the number of nonzero ϱ_{jk}'s exceeds a certain threshold value. The idea of using a relative distance is similar to the Cucker-Smale method,[5] although the proposed distance-based connectivity method does not directly affect the stability condition as shown in Section V.

C. Adaptation of Diffusive Coupling Gains

In addition to the nominal gains (k_1, k_2), there are different types of gains for the jth agent with the kth agent: c_{jj} and c_{jk}, obtained by the adaptation law in this section. The matrix $\mathcal{W}_j(\mathbf{u}'_{\rm tr}, \boldsymbol{\varrho}_j) \in \mathbb{R}^{3\times p}$ and the vector $\mathbf{c}_j \in \mathbb{R}^{p\times 1}$ are defined as

$$\begin{aligned} \mathcal{W}_j(\mathbf{u}'_{\rm tr}, \boldsymbol{\varrho}_j) &:= [\varrho_{j1}\mathbf{u}'_{1,\rm tr} \,\vdots\, \varrho_{j2}\mathbf{u}'_{2,\rm tr} \,\vdots\, \cdots \,\vdots\, \varrho_{jp}\mathbf{u}'_{p,\rm tr}] \\ \mathbf{c}_j &:= [c_{j1}, c_{j2}, \cdots, c_{jp}]^T \end{aligned} \tag{26}$$

where $\mathbf{c}_j$ is a vector whose elements are the tracking and diffusive coupling gains for the jth agent. For example, $c_{jk}\mathbf{u}'_{k,\rm tr} = c_{jk}\mathbf{u}'_{j,\rm tr} + c_{jk}(\mathbf{u}'_{k,\rm tr} - \mathbf{u}'_{j,\rm tr})$.

We propose the coupling gain adaptation law that adjusts the values of $\mathbf{c}_j$ so that the graph Laplacians is automatically changed by the current state errors, synchronization errors, and the distance-based connectivity.

$$\dot{\mathbf{c}}_j = \boldsymbol{\Sigma}_j \text{Proj}\left(\mathbf{c}_j,\ \mathcal{W}_j^T(\mathbf{u}'_{\rm tr}, \boldsymbol{\varrho}_j)\mathbf{u}'_{j,\rm tr}\right) - \boldsymbol{\Sigma}_j \mathbf{S}_{\mathbf{c}_j}(\mathbf{c}_j)\mathbf{c}_j \tag{27}$$

where $\text{Proj}(\cdot,\cdot)$ denotes the projection method with smooth transition from the original vector field to a tangent vector field,[22].[15] Also, $\boldsymbol{\Sigma}_j = \text{diag}(\sigma_{j1},\ \sigma_{j2}, \cdots, \sigma_{jp}) > 0$. Each element of the $p \times p$ diagonal matrix $\mathbf{S}_{\mathbf{c}_j}$ is some positive constant $\ell_k > 0$, $(1 \le k \le p)$ if $|c_{j,k}| > c_{\max,j,k}$, where $c_{\max,j,k}$ is the maximum allowable $|c_{j,k}|$, or if $\varrho_{jk}(d_{jk}) = 0$. Otherwise, it is zero.

Remark 5 $\mathcal{W}_j$ is a function of $\varrho_{jk}(d_{jk})$ in (24) as well as $\mathbf{u}'_{\rm tr}$. If the relative distance between the jth and kth agents exceeds $d_{\rm limit}$, the kth element in $\mathcal{W}_j$ becomes zero due to $\varrho_{jk}(d_{jk}) = 0$. Then, the corresponding coupling gain c_{jk} will not be updated and exponentially tends to zero due to the damping term in (27).

D. Adaptation for Parametric Uncertainties

The estimated parameters $\hat{\mathbf{b}}_j \in \mathbb{R}^l$ of (1) are adapted by

$$\begin{aligned} \dot{\hat{\mathbf{b}}}_j &= -\boldsymbol{\Gamma}_j \text{Proj}\Big(\hat{\mathbf{b}}_j,\ \mathcal{Y}_j^T(\mathbf{q}'_j, \dot{\mathbf{q}}'_j, \dot{\mathbf{q}}'_{j,r}, \ddot{\mathbf{q}}'_{j,r})\mathbf{u}'_j\Big) \\ &\quad -\boldsymbol{\Gamma}_j \mathbf{S}_{\hat{\mathbf{b}}_j}(\hat{\mathbf{b}}_j)\Big(\hat{\mathbf{b}}_j + \text{sgn}(\hat{\mathbf{b}}_j)\mathbf{b}_{\max}\Big) \end{aligned} \tag{28}$$

where $\mathbf{b}_{\max}$ represents both the boundary of the projection operator $\text{Proj}(\hat{\mathbf{b}}_j, \mathcal{Y}_j^T\mathbf{u}'_j)$ and the known maximum value of the true unknown value $\mathbf{b}$. Also,

$$\begin{bmatrix} \mathcal{Y}_j \\ \mathcal{Y}_{jZ'} \end{bmatrix} \tilde{\mathbf{b}}_j =: \mathbf{T}_{j-1}^T \begin{bmatrix} \mathbf{Y}_j(\mathbf{q}'_j, \dot{\mathbf{q}}'_j, \dot{\mathbf{q}}'_{j,r}, \ddot{\mathbf{q}}'_{j,r}) \\ Y_{jZ'} \end{bmatrix} \tilde{\mathbf{b}}_j \tag{29}$$

where $\mathbf{Y}_j\hat{\mathbf{b}}_j = \mathbf{R}_{\rm f}\hat{\mathbf{M}}_j\mathbf{R}_{\rm f}^T\ddot{\mathbf{q}}'_{j,r} + \mathbf{R}_{\rm f}\hat{\mathbf{C}}_j\mathbf{R}_{\rm f}^T\dot{\mathbf{q}}'_{j,r} + \mathbf{R}_{\rm f}\hat{\mathbf{D}}_j$ and $Y_{jZ'}\hat{\mathbf{b}}_j = Y_{j,3}\hat{\mathbf{b}}_j \cot(\psi + \Phi)$ from (22) and $Y_{j,3}$ is the third row vector of $\mathbf{Y}_j$ (see (16)). Also, $\boldsymbol{\Gamma}_j = \text{diag}(\gamma_{j1},\ \gamma_{j2}, \cdots, \gamma_{jl})$ is an $l \times l$ positive diagonal matrix for the jth agent. Each diagonal element of the $l \times l$ diagonal matrix $\mathbf{S}_{\hat{\mathbf{b}}_j}(\hat{\mathbf{b}}_j)$ is some positive constant ς_k, $(1 \le k \le l)$ only if $|\hat{b}_{j,k}| > b_{\max,k}$. Otherwise, it is zero. Each element $b_{\max,k} > 0$ in $\mathbf{b}_{\max}$ is greater than the corresponding elements $|b_{j,k}|$ in $\mathbf{b}_j$ $(1 \le j \le p)$. The $l \times l$ diagonal matrix $\text{sgn}(\hat{\mathbf{b}}_j)$ has a sign function of each element of $\hat{\mathbf{b}}_j$ as its diagonal entries.

E. Collision Avoidance for Reconfiguration

We introduce a method of collision-avoidance that can be integrated with the main controller in (22). While the phase difference on an ellipse already implies collision avoidance, the method in this section considers the transient maneuvers (e.g., reconfiguration from arbitrary initial positions). Suppose that there is a collision surface radius $r_{{\rm col},j}$ for the jth vehicle. If the relative distance between jth and kth vehicles d_{jk} is less than the collision surface radius, i.e., $d_{jk} < r_{{\rm col},j}$, $\mathbf{Q}_{j,\rm tr}$ for the jth vehicle in (22) is activated as:

$$\mathbf{Q}_{j,\rm tr} = k_{\mathbf{Q}_j} \sum_{j\neq k; d_{jk} < r_{{\rm col},j}} \|\dot{\mathbf{q}}_{j,\rm tr}\| \|\dot{\mathbf{q}}_{k,\rm tr}\| \sin(\theta_{jk}/2)\hat{\mathbf{n}}_{jk} \tag{30}$$

where $\theta_{jk} = \cos^{-1}\left(\frac{\dot{\mathbf{q}}_{j,\mathrm{tr}}\cdot\dot{\mathbf{q}}_{k,\mathrm{tr}}}{\|\dot{\mathbf{q}}_{j,\mathrm{tr}}\|\|\dot{\mathbf{q}}_{k,\mathrm{tr}}\|}\right)$ and $k_{\mathbf{Q}_j} > 0$ denote design parameters determining the size of collision avoidance area. Also, $\hat{\mathbf{n}}_{jk}$ denotes a unit vector:

$$\hat{\mathbf{n}}_{jk} = \begin{cases} \dot{\mathbf{q}}_{j,\mathrm{tr}} \times \dot{\mathbf{q}}_{\mathrm{p,tr}}/\|\dot{\mathbf{q}}_{j,\mathrm{tr}}\|, & \text{if } \theta_{jk} = \pi \\ \dot{\mathbf{q}}_{j,\mathrm{tr}} \times \dot{\mathbf{q}}_{k,\mathrm{tr}}/(\|\dot{\mathbf{q}}_{j,\mathrm{tr}}\|\|\dot{\mathbf{q}}_{k,\mathrm{tr}}\|), & \text{otherwise} \end{cases} \tag{31}$$

where $\dot{\mathbf{q}}_{\mathrm{p,tr}}$ is a unit vector which is not parallel to other velocities when considering collisions. Notice that $\mathbf{Q}_{j,\mathrm{tr}}$ is activated only when $d_{jk} < r_{\mathrm{col},j}$, which is smaller than nominal separation distances on ellipses.

V. Main Results of Stability Analysis

A. Closed-Loop Models of Networked EL Systems

Suppose that there are p agents in the network. Then from (21), (22) and (23), the jth closed-loop system is

$$\begin{aligned} &\begin{bmatrix} \mathbf{R}_{\mathrm{f}}\mathbf{M}_j(\mathbf{q}_j)\mathbf{R}_{\mathrm{f}}^T & \mathbf{0}_{n\times 1} \\ \mathbf{0}_{1\times n} & (\mathbf{R}_{\mathrm{f}}\mathbf{M}_j(\mathbf{q}_j)\mathbf{R}_{\mathrm{f}}^T)_{n,n} \end{bmatrix}\dot{\mathbf{s}}_j'' \\ &+\begin{bmatrix} \mathbf{R}_{\mathrm{f}}\mathbf{C}_j(\mathbf{q}_j,\dot{\mathbf{q}}_j)\mathbf{R}_{\mathrm{f}}^T & \mathbf{0}_{n\times 1} \\ \mathbf{0}_{1\times n} & (\mathbf{R}_{\mathrm{f}}\mathbf{C}_j(\mathbf{q}_j,\dot{\mathbf{q}}_j)\mathbf{R}_{\mathrm{f}}^T)_{n,n} \end{bmatrix}\mathbf{s}_j'' \\ &-\begin{bmatrix} \mathbf{Y}_j(\mathbf{q}_j',\dot{\mathbf{q}}_j',\dot{\mathbf{q}}_{j,r}',\ddot{\mathbf{q}}_{j,r}') \\ Y_{jZ'} \end{bmatrix}\tilde{\mathbf{b}}_j + \begin{bmatrix} \mathbf{0}_{(n-3)\times 1} \\ \mathbf{T}_{j-1}'\mathcal{W}_j\mathbf{c}_j \end{bmatrix} \\ &+\begin{bmatrix} k_0\mathbf{s}_{j,\mathrm{other}}'' \\ k_1\mathbf{s}_{j,\mathrm{tr}}'' \end{bmatrix} - \begin{bmatrix} \mathbf{0}_{(n-3)\times 1} \\ k_2\left(\mathbf{T}_{j-l}'\mathbf{s}_{l,\mathrm{tr}}'' + \mathbf{T}_{j-m}'\mathbf{s}_{m,\mathrm{tr}}''\right) \end{bmatrix} = \begin{bmatrix} \boldsymbol{\Delta}_{\mathrm{dist},j} \\ \Delta_{jZ'} \end{bmatrix} \end{aligned} \tag{32}$$

where $\tilde{\mathbf{b}}_j \in \mathbb{R}^l$ is defined as $\tilde{\mathbf{b}}_j := \hat{\mathbf{b}}_j - \mathbf{b}_j$ where $\mathbf{b}_j$ is assumed to be constant or slowly varying so that $\dot{\tilde{\mathbf{b}}}_j = \dot{\hat{\mathbf{b}}}_j - \dot{\mathbf{b}}_j = \dot{\hat{\mathbf{b}}}_j$. Also, $\boldsymbol{\Delta}_{\mathrm{dist},j}$ denotes a non-vanishing disturbance that might include a nonzero $\dot{\mathbf{b}}_j$.

In order to show the motion synchronization, the composite variable $\mathbf{s}_j''$ has to be rotated by $\mathbf{T}_{j-1}^T = \mathbf{T}^T((j-i)\phi)$ so that $\mathbf{s}_j''$ can be directly compared with $\mathbf{s}_1''$.[2] Therefore, rewriting $\mathbf{s}_j''$ by $\mathbf{T}_{j-1}\mathbf{T}_{j-1}^T\mathbf{s}_j''$ and pre-multiplying (32) by $\mathbf{T}_{j-1}^T$ results in

$$\begin{aligned} &\underbrace{\left(\mathbf{T}_{j-1}^T\begin{bmatrix} \mathbf{R}_{\mathrm{f}}\mathbf{M}_j(\mathbf{q}_j)\mathbf{R}_{\mathrm{f}}^T & \mathbf{0}_{n\times 1} \\ \mathbf{0}_{1\times n} & (\mathbf{R}_{\mathrm{f}}\mathbf{M}_j(\mathbf{q}_j)\mathbf{R}_{\mathrm{f}}^T)_{n,n} \end{bmatrix}\mathbf{T}_{j-1}\right)}_{=:\,\mathcal{M}_j''(\mathbf{q}_j)}\mathbf{T}_{j-1}^T\dot{\mathbf{s}}_j'' \\ &+\underbrace{\left(\mathbf{T}_{j-1}^T\begin{bmatrix} \mathbf{R}_{\mathrm{f}}\mathbf{C}_j(\mathbf{q}_j,\dot{\mathbf{q}}_j)\mathbf{R}_{\mathrm{f}}^T & \mathbf{0}_{n\times 1} \\ \mathbf{0}_{1\times n} & (\mathbf{R}_{\mathrm{f}}\mathbf{C}_j(\mathbf{q}_j,\dot{\mathbf{q}}_j)\mathbf{R}_{\mathrm{f}}^T)_{n,n} \end{bmatrix}\mathbf{T}_{j-1}\right)}_{=:\,\mathcal{C}_j''(\mathbf{q}_j,\dot{\mathbf{q}}_j)}\mathbf{T}_{j-1}^T\mathbf{s}_j'' \\ &-\mathbf{T}_{j-1}^T\begin{bmatrix} \mathbf{Y}_j(\mathbf{q}_j',\dot{\mathbf{q}}_j',\dot{\mathbf{q}}_{j,r}',\ddot{\mathbf{q}}_{j,r}') \\ Y_{jZ'} \end{bmatrix}\tilde{\mathbf{b}}_j + \begin{bmatrix} \mathbf{0}_{(n-3)\times 1} \\ \mathcal{W}_j(\mathbf{u}_{\mathrm{tr}}',\boldsymbol{\varrho}_j)\mathbf{c}_j \end{bmatrix} \\ &+\begin{bmatrix} k_0\mathbf{s}_{j,\mathrm{other}}'' \\ k_1\mathbf{T}_{j-1}'^T\mathbf{s}_{j,\mathrm{tr}}'' \end{bmatrix} - \begin{bmatrix} \mathbf{0}_{(n-3)\times 1} \\ k_2\left(\mathbf{T}_{l-1}'^T\mathbf{s}_{l,\mathrm{tr}}'' + \mathbf{T}'^T_{m-1}\mathbf{s}_{m,\mathrm{tr}}''\right) \end{bmatrix} \\ &=\mathbf{T}_{j-1}^T\begin{bmatrix} \boldsymbol{\Delta}_{\mathrm{dist},j} \\ \Delta_{jZ'} \end{bmatrix} =: \begin{bmatrix} \boldsymbol{\Delta}_{\mathrm{dist},j}' \\ \Delta_{jZ'}' \end{bmatrix} \end{aligned} \tag{33}$$

It might appear as if the dynamic model had $(n+1)$ independent variables in (33). However, the $(n+1)$th variable is just an auxiliary variable, which can be obtained directly from the original ones. Hence, (33) can be rewritten by using the variables with one prime:

$$\begin{aligned} &\mathcal{M}_j'(\mathbf{q}_j)\dot{\mathbf{u}}_j' + \mathcal{C}_j'(\mathbf{q}_j,\dot{\mathbf{q}}_j)\mathbf{u}_j' - \mathcal{Y}_j(\mathbf{q}_j',\dot{\mathbf{q}}_j',\dot{\mathbf{q}}_{j,r}',\ddot{\mathbf{q}}_{j,r}')\tilde{\mathbf{b}}_j \\ &+\begin{bmatrix} k_0\mathbf{u}_{j,\mathrm{other}}' \\ k_1\mathbf{u}_{j,\mathrm{tr}}' - k_2\left(\mathbf{u}_{l,\mathrm{tr}}' + \mathbf{u}_{m,\mathrm{tr}}'\right) + \mathcal{W}_j(\mathbf{u}_{\mathrm{tr}}',\boldsymbol{\varrho}_j)\mathbf{c}_j \end{bmatrix} = \boldsymbol{\Delta}'_{\mathrm{dist},j} \end{aligned} \tag{34}$$

where $\mathbf{u}_j' = [\mathbf{u}_{j,\mathrm{other}}'; \mathbf{u}_{j,\mathrm{tr}}']$ as defined in (18). Also, $\mathcal{M}_j' \in \mathbb{R}^{n\times n}$ and $\mathcal{C}_j' \in \mathbb{R}^{n\times n}$ are the first $n\times n$ matrices taken from $\mathcal{M}_j'' \in \mathbb{R}^{(n+1)\times(n+1)}$ and $\mathcal{C}_j'' \in \mathbb{R}^{(n+1)\times(n+1)}$: $\mathcal{M}_j' = \mathcal{M}_{j,\mathrm{other}}' \oplus \mathcal{M}_{j,\mathrm{tr}}'$ and $\mathcal{C}_j' = \mathcal{C}_{j,\mathrm{other}}' \oplus \mathcal{C}_{j,\mathrm{tr}}'$.

The coupled dynamic models, obtained by concatenating each component from the closed-loop system

(34), the coupling gain adaptation law (27) and the parameter estimation law (28), can be written as

$$\begin{bmatrix} [\mathcal{M}'] & \mathbf{0} & \mathbf{0} \\ \mathbf{0} & [\mathbf{\Sigma}^{-1}] & \mathbf{0} \\ \mathbf{0} & \mathbf{0} & [\mathbf{\Gamma}^{-1}] \end{bmatrix} \begin{bmatrix} \dot{\mathbf{u}}' \\ \{\dot{\mathbf{c}}\} \\ \{\dot{\tilde{\mathbf{b}}}\} \end{bmatrix} + \begin{bmatrix} [\mathcal{C}']+[\mathbf{L}] & \begin{bmatrix} \mathbf{0} \\ [\mathcal{W}] \end{bmatrix} & -[\mathcal{Y}] \\ \begin{bmatrix} \mathbf{0} & -[\mathcal{W}]^T \end{bmatrix} & [\mathbf{S_c}] & \mathbf{0} \\ [\mathcal{Y}]^T & \mathbf{0} & [\mathbf{S}_{\tilde{\mathbf{b}}}] \end{bmatrix} \begin{bmatrix} \mathbf{u}' \\ \{\mathbf{c}\} \\ \{\tilde{\mathbf{b}}\} \end{bmatrix} = \begin{bmatrix} \{\mathbf{\Delta}'_{\text{dist}}\} \\ \{\mathrm{P_c}\} \\ \{\mathrm{P_b}\}-[\mathbf{S}_{\hat{\mathbf{b}}}]\{\mathbf{b}_r\} \end{bmatrix} \tag{35}$$

where $\mathbf{u}' = [\mathbf{u}'_{\text{other}}; \mathbf{u}'_{\text{tr}}]$ with $\mathbf{u}'_{\text{tr}} = [\mathbf{u}'_{1,\text{tr}}; \cdots; \mathbf{u}'_{p,\text{tr}}]$, and $\mathbf{u}'_{\text{other}} = [\mathbf{u}'_{1,\text{other}}; \cdots; \mathbf{u}'_{p,\text{other}}]$. Also, $[\mathcal{M}'] = [\mathcal{M}']_{\text{other}} \oplus [\mathcal{M}']_{\text{tr}}$ with $[\mathcal{M}']_{\text{other}} = \mathcal{M}'_{1,\text{other}} \oplus \cdots \oplus \mathcal{M}'_{p,\text{other}}$ and $[\mathcal{M}']_{\text{tr}} = \mathcal{M}'_{1,\text{tr}} \oplus \cdots \oplus \mathcal{M}'_{p,\text{tr}}$. Similarly, the block diagonal matrices $[\mathcal{C}']$, $[\mathcal{Y}]$ and $[\mathcal{W}]$ are defined. Note that $\{\mathrm{P_c}\} = \{\mathrm{P_c}(\mathbf{c}, \mathbf{c})\}$ and $\{\mathrm{P_b}\} = \{\mathrm{P_b}(\hat{\mathbf{b}}, \hat{\mathbf{b}})\}$ where

$$\begin{aligned} \{\mathrm{P_c}(\mathbf{c}, \mathbf{y})\} &= \{\mathrm{Proj}(\mathbf{c}, \mathbf{y}, \mathcal{W}^T \mathbf{u}'_{\text{tr}})\} - [\mathcal{W}]^T \mathbf{u}'_{\text{tr}} \\ \{\mathrm{P_b}(\hat{\mathbf{b}}, \mathbf{y})\} &= \{\mathrm{Proj}(\hat{\mathbf{b}}, \mathbf{y}, -\mathcal{Y}^T \mathbf{u}')\} + [\mathcal{Y}]^T \mathbf{u}' \\ \{\mathbf{b}_r\} &= \{\mathbf{b}\} + [\mathrm{sgn}(\{\hat{\mathbf{b}}\})]\{\mathbf{b}_{\max}\} \end{aligned} \tag{36}$$

and $\mathrm{Proj}(\boldsymbol{\theta}, \mathbf{y}, \mathbf{x}) = \mathbf{x} - \frac{\nabla f(\mathbf{y}) \nabla f(\boldsymbol{\theta})^T}{\|\nabla f(\boldsymbol{\theta})\|^2} \mathbf{x} f(\boldsymbol{\theta})$ if $f(\boldsymbol{\theta}) > 0$ and $\nabla f(\boldsymbol{\theta})^T \mathbf{x} > 0$ for a boundary function $f(\boldsymbol{\theta})$. Otherwise, $\mathrm{Proj}(\boldsymbol{\theta}, \mathbf{y}, \mathbf{x}) = \mathbf{x}$. This additional argument of $\mathbf{y}$ will be used in Sect. V for stability analysis.

Definition 1 *The closed-loop system (35) has the adaptive graph Laplacian matrix* $[\mathbf{L}]_a \in \mathbb{R}^{np \times np}$ *defined as*

$$[\mathbf{L}]_a := [\mathbf{L}] + [\mathbf{c}] = k_0 \mathbf{I}_{(n-3)p} \oplus ([\mathbf{L}]_{\text{tr}} + [\mathbf{c}]_{\text{tr}}) \tag{37}$$

where $[\mathbf{L}] = k_0 \mathbf{I}_{(n-3)p} \oplus [\mathbf{L}]_{\text{tr}}$ *and* $[\mathbf{c}] = \mathbf{0}_{(n-3)\times p} \oplus [\mathbf{c}]_{\text{tr}}$. *The nominal Laplacian matrix* $[\mathbf{L}]_{\text{tr}}$, *defined from the main control law (22) with bidirectional couplings, is chosen such that* $[\mathbf{L}]_{\text{tr}} > 0$. *Notice that we used*

$$[\mathcal{W}(\mathbf{u}'_{\text{tr}}, \boldsymbol{\varrho})]\{\mathbf{c}\} = [\mathbf{c}]_{\text{tr}} \mathbf{u}'_{\text{tr}} \tag{38}$$

Hence, each element of the matrix $[\mathbf{c}]_{\text{tr}}$ *defines an adaptive tracking/diffusive coupling gain weighted by the distance-based connectivity function in (24) such that*

$$[\mathbf{c}]_{\text{tr}} := \begin{bmatrix} \varrho_{11} c_{11} & \varrho_{12} c_{12} & \cdots & \varrho_{1p} c_{1p} \\ \varrho_{21} c_{21} & \varrho_{22} c_{22} & \cdots & \varrho_{2p} c_{2p} \\ \vdots & \vdots & \ddots & \vdots \\ \varrho_{p1} c_{p1} & \varrho_{p2} c_{p2} & \cdots & \varrho_{pp} c_{pp} \end{bmatrix} \otimes \mathbf{I}_3 \tag{39}$$

where the number of nonzero entries for each column equals $m_n + 1$ *where* m_n *denotes the maximum allowable number of communication neighbors. Hence,* $\|[\mathbf{c}]_{\text{tr}}\|_\infty \leq c_{\max}(m_n + 1)$ *with* $|\mathbf{c}_{\max,j,k}| \leq c_{\max}$, $\forall j, k$. *Note that* $[\mathbf{c}]_{\text{tr}}$ *is not a symmetric matrix since* c_{ij} *need not equal* c_{ji}.

Remark 6 Since the system is nominally on a regular bidirectional graph, as studied in,[3] the symmetric positive definite matrix $\lambda_{\min}([\mathbf{L}]_{\text{tr}}) = k_1 - 2k_2 > 0$ if $k_1(t) > 2k_2(t) > 0$, $\forall t$ for $p \geq 3$.

Remark 7 The gain adaptation $[\mathbf{c}]_{\text{tr}}$ in the adaptive Laplacian matrix in (37) considers translational motions due to the focus on elliptical motions. However, (22) can be modified such that coupling connections exist for other generalized coordinates $\mathbf{u}'_{\text{other}}$[2,3] (i.e., $[\mathbf{L}]_a$ in (37) has off-diagonal terms for every row).

B. Main Stability Proof

We present the stability proof of the closed-loop system.

Lemma 3 Contraction Analysis.[16] *Suppose there is a smooth nonlinear non-autonomous system* $\dot{\mathbf{x}}(t) = \mathbf{f}(\mathbf{x}(t), t)$ *where* $\mathbf{x}(t) \in \mathbb{R}^n$. *A virtual displacement* $\delta\mathbf{x}$ *is defined as an infinitesimal displacement at fixed time, and* $\mathbf{\Theta}(\mathbf{x}, t)$ *is a smooth coordinate transformation of the virtual displacement such that* $\delta\mathbf{z} = \mathbf{\Theta}\delta\mathbf{x}$. *Then if there exists a positive* λ *and a uniformly positive definite metric,* $\mathbf{M}(\mathbf{x}, t) = \mathbf{\Theta}(\mathbf{x}, t)^T \mathbf{\Theta}(\mathbf{x}, t)$, *such that*

$$\begin{aligned} &\frac{d}{dt}\Big(\delta\mathbf{z}^T \delta\mathbf{z}\Big) = \frac{d}{dt}\Big(\delta\mathbf{x}^T \mathbf{M}(\mathbf{x}, t) \delta\mathbf{x}\Big) \\ &= \delta\mathbf{x}^T \Big(\dot{\mathbf{M}} + \Big(\frac{\partial \mathbf{f}}{\partial \mathbf{x}}\Big)^T \mathbf{M} + \mathbf{M} \frac{\partial \mathbf{f}}{\partial \mathbf{x}}\Big) \delta\mathbf{x} \leq -2\lambda \delta\mathbf{x}^T \mathbf{M}(\mathbf{x}, t) \delta\mathbf{x} \end{aligned} \tag{40}$$

Then all system trajectories converge exponentially fast to a single trajectory regardless of the initial conditions ($\delta\mathbf{z},\ \delta\mathbf{x} \to \mathbf{0}$), i.e., contracting at a rate of λ. The proof[16] immediately follows from the exponential stability of $\|\delta\mathbf{z}\| = \sqrt{\delta\mathbf{z}^T\delta\mathbf{z}}$, which is deduced from (40).

Lemma 3 is very useful for proving the stability of EL systems. Note that the inertia matrix $\mathbf{M}_j(\mathbf{q}_j)$ in (1) can be chosen as the metric $\mathbf{M}(\mathbf{x},t)$ in (40). For example, consider an observer-like virtual system of $\mathbf{M}(\mathbf{q})\dot{\mathbf{y}} + \mathbf{C}(\mathbf{q},\dot{\mathbf{q}})\mathbf{y} + \mathbf{K}\mathbf{y} = \mathbf{0}$ with two particular solutions $\mathbf{y} = \mathbf{0}$ and $\mathbf{y} = \mathbf{s}$, where $\mathbf{s}$ is some composite variable similar to (17). By regarding the virtual dynamics as only functions of $\mathbf{y}$, i.e., $\mathbf{M}(\mathbf{q}) = \mathbf{M}(t)$, we can straightforwardly prove the global exponential stability of the system. Then, the stability of $\mathbf{q}$ can be deduced from $\mathbf{s}$ in a hierarchical fashion, as shall be seen in the next lemma. If we use Lyapunov stability theory instead, we often need to use an ad-hoc Lyapunov function with a cross-term (e.g., $V = \mathbf{s}^T\mathbf{M}(\mathbf{q})\mathbf{s} + \tilde{\mathbf{q}}^T\tilde{\mathbf{q}} + \alpha\mathbf{s}^T\mathbf{M}(\mathbf{q})\tilde{\mathbf{q}}$, $\exists\alpha$).

Lemma 4 Contraction & Robustness.[16] *Consider a nonlinear non-autonomous system $\dot{\mathbf{x}} = \mathbf{f}(\mathbf{x},t)$ which is contracting with a contraction rate λ. Let $P_1(t)$ be a trajectory of the system. If there exists a perturbed system $\dot{\mathbf{x}} = \mathbf{f}(\mathbf{x},t) + \mathbf{d}(\mathbf{x},t)$ and its trajectory $P_2(t)$, then the distance $R(t) = \int_{P_2}^{P_1}\|\delta\mathbf{z}(t)\|$ satisfies $\forall t \geq t_0$*

$$\begin{aligned} &R(t) \leq e^{-\lambda(t-t_0)}R(t_0) + \frac{1-e^{-\lambda(t-t_0)}}{\lambda}\sup_{\mathbf{x},t}\|\mathbf{\Theta}\mathbf{d}\|, \\ &\textit{and, as } t\to\infty,\ R(t) \leq \sup_{\mathbf{x},t}\|\mathbf{\Theta}(\mathbf{x},\mathbf{t})\mathbf{d}(\mathbf{x},t)\|\lambda \end{aligned} \tag{41}$$

Proof: After differentiating $R(t) = \int_{P_2}^{P_1}\|\delta\mathbf{z}(t)\|$, we can obtain $\dot{R} + \lambda R \leq \|\mathbf{\Theta}\mathbf{d}\|$. Then, we can apply the comparison lemma [13, p.102-103, p. 350-353] to estimate the bound of $R(t)$. ■

Equivalently, we can compute an ultimate bound, which is true for $t \geq t_0 + T$, $\exists T$ instead of $t\to\infty$ as in Lemma 4, since a globally exponentially stable system is input-to-state stable (ISS).[13]

Lemma 5 Robust Hierarchical Connection.[16] *The hierarchically combined system with a generalized Jacobian matrix $\left[\begin{smallmatrix}\mathbf{F}_{11} & \mathbf{0}\\ \mathbf{F}_{21} & \mathbf{F}_{22}\end{smallmatrix}\right]$ is assumed to be subject to a perturbed flow field of $[\mathbf{d}_1;\mathbf{d}_2]$. Then, the path length integral $R_i(t) = \int_{P_1}^{P_2}\|\delta\mathbf{z}_i\|$, $i = 1,2$ between the original and perturbed dynamics can be written as*

$$\begin{aligned} &\dot{R}_1 + |\lambda_{max}(\mathbf{F}_{11})|R_1 \leq \|\mathbf{\Theta}_1\mathbf{d}_1\| \\ &\dot{R}_2 + |\lambda_{max}(\mathbf{F}_{22})|R_2 \leq \|\mathbf{\Theta}_2\mathbf{d}_2\| + \int_{P_1}^{P_2}\|\mathbf{F}_{21}\|\|\delta\mathbf{z}_1\| \end{aligned} \tag{42}$$

Theorem 6 *The coupled EL systems (35) globally exponentially converge to their desired trajectories with bounded errors such that the distance $R_2(t) = \int_{\mathbf{q}_d'(t)}^{(\mathbf{T}_{j-1}^T\mathbf{q}_j'')'}\|\delta\mathbf{z}\|$ between each $[\mathbf{I}_n\mathbf{0}_{n\times 1}]\mathbf{T}_{j-1}^T\mathbf{q}_j''$ and the desired trajectory $\mathbf{q}_d'(t)$ exponentially tends to the following ball with a contraction rate of $k_0/\lambda_{\max}(\mathbf{H}(\mathbf{q}))$*

$$R_2(t) \leq \frac{\lambda_{\max}(\mathbf{H}(\mathbf{q}))}{\lambda'' k_0\lambda_{\min}(\mathbf{H}(\mathbf{q}))}\left(\|\{\mathbf{\Delta}_{\text{dist}}\}\| + \|[\mathcal{Y}]\{\tilde{\mathbf{b}}\}\|\right) \tag{43}$$

*where $\lambda'' > 0$ is from $\mathbf{s}_j''$ in (17) and $[\mathbf{H}(\mathbf{q})] = [\mathcal{M}'(\mathbf{q})] \oplus [\mathbf{\Sigma}^{-1}]_o \oplus [\mathbf{\Gamma}^{-1}]_o$, **if** the time-varying gains $(k_1(t) - 2k_2(t) > 0, k_2(t) > 0,\ \forall t)$ verify*

$$k_1(t) - 2k_2(t) = k_0 - \lambda_{\min}\left(\frac{[\mathbf{c}(t)]_{\text{tr},i} + [\mathbf{c}(t)]_{\text{tr},i}^T}{2}\right) \tag{44}$$

as well as $\lambda_{\min}([\mathbf{S}_{\hat{\mathbf{b}}}]) \geq k_0$ and $\lambda_{\min}([\mathbf{S}_{\mathbf{c}}]) \geq k_0$.

Proof: Previously, we obtained the closed-loop dynamic model for p agents in (35), each of which has p adaptive coupling gains and l unknown physical parameters. We further analyze the system based on the location of the elements in $\{\mathbf{c}\}$ and $\{\tilde{\mathbf{b}}\}$.

$$\{\mathbf{c}\} = \begin{bmatrix}\{\mathbf{c}\}_o\\ \{\mathbf{c}\}_i\end{bmatrix}, \quad \{\tilde{\mathbf{b}}\} = \begin{bmatrix}\{\tilde{\mathbf{b}}\}_o\\ \{\tilde{\mathbf{b}}\}_i\end{bmatrix} \tag{45}$$

where the subscript o and i denote the concatenation of the states located outside and inside their boundaries of the projection operator, respectively. Since the exponential convergence of $\{\mathbf{c}\}_i$ and $\{\tilde{\mathbf{b}}\}_i$ cannot be guaranteed, we regard them as disturbances. Then, (35) becomes

$$
\begin{aligned}
[\mathbf{H}(\mathbf{q})]\begin{bmatrix}\dot{\mathbf{u}}'\\ \{\dot{\mathbf{c}}\}_o\\ \{\dot{\tilde{\mathbf{b}}}\}_o\end{bmatrix} + \underbrace{\begin{bmatrix}[\mathcal{C}']+[\mathbf{L}] & \begin{bmatrix}\mathbf{0}\\ [\mathcal{W}]_o\end{bmatrix} & -[\mathcal{Y}]_o\\ \begin{bmatrix}\mathbf{0} & -[\mathcal{W}]_o^T\end{bmatrix} & [\mathbf{S_c}]_o & \mathbf{0}\\ [\mathcal{Y}]_o^T & \mathbf{0} & [\mathbf{S}_{\tilde{\mathbf{b}}}]_o\end{bmatrix}}_{=:\mathbf{Q}(\mathbf{q},\dot{\mathbf{q}},\mathbf{u}')}\begin{bmatrix}\mathbf{u}'\\ \{\mathbf{c}\}_o\\ \{\tilde{\mathbf{b}}\}_o\end{bmatrix}\\
= \begin{bmatrix}\{\boldsymbol{\Delta}'_{\text{dist}}\} - \begin{bmatrix}\mathbf{0}\\ [\mathcal{W}]_i\end{bmatrix}\{\mathbf{c}\}_i + [\mathcal{Y}]_i\{\tilde{\mathbf{b}}\}_i\\ \{\mathrm{P}_{\mathbf{c}}\}_o\\ \{\mathrm{P}_{\mathbf{b}}\}_o - [\mathbf{S}_{\tilde{\mathbf{b}}}]_o\{\mathbf{b}_r\}_o\end{bmatrix}
\end{aligned}
\tag{46}
$$

where $[\mathbf{L}] = k_0\mathbf{I}_{(n-3)p} \oplus [\mathbf{L}]_{\text{tr}}$ from (37).

An observer-like virtual system of $\mathbf{y} = (\mathbf{y}_1; \mathbf{y}_2; \mathbf{y}_3)$ for (46) can be written as

$$
\begin{aligned}
&[\mathbf{H}(\mathbf{q})]\,\dot{\mathbf{y}} + [\mathbf{Q}((\mathbf{q}, \dot{\mathbf{q}}, \mathbf{u}'))]\mathbf{y} + [\mathbf{c}]_i\,\mathbf{y}_1 \\
&- \begin{bmatrix}\mathbf{0}\\ \{\mathrm{P}_{\mathbf{c}}(\mathbf{c}, \mathbf{y}_2)\}_o\\ \{\mathrm{P}_{\mathbf{b}}(\hat{\mathbf{b}}, \mathbf{y}_3 + \mathbf{b})\}_o - [\mathbf{S}_{\tilde{\mathbf{b}}}]_o\{\mathbf{b}_r\}_o\end{bmatrix} = \begin{bmatrix}\{\boldsymbol{\Delta}'_{\text{dist}}\} + [\mathcal{Y}]_i\{\tilde{\mathbf{b}}\}_i\\ \mathbf{0}\\ \mathbf{0}\end{bmatrix}
\end{aligned}
\tag{47}
$$

where we used $[\,\mathbf{0};\, [\mathcal{W}]_i\,]\,\{\mathbf{c}\}_i = [\mathbf{c}]_{\text{tr},i}\mathbf{u}'_{\text{tr}}$. Also, $\{\mathrm{P}_{\mathbf{c}}(\mathbf{c}, \mathbf{y}_2)\}$, $\{\mathrm{P}_{\mathbf{b}}(\hat{\mathbf{b}}, \mathbf{y}_3 + \mathbf{b})\}$, and $\{\mathbf{b}_r\}$ are given in (36).

By comparing (46) and (47), we can find that this virtual system has the following particular solution: $\mathbf{y}_1 = \mathbf{u}'$ defined from (19), $\mathbf{y}_2 = \{\mathbf{c}\}_o$, $\mathbf{y}_3 = \{\tilde{\mathbf{b}}\}_o$. Obviously, $\mathbf{y}_1 = \mathbf{0}$ is not a solution of (47), in contrast with its unperturbed system that is obtained by setting the righthand side (RHS) of (47) zero. We define a squared virtual length $V := \delta\mathbf{y}^T[\mathbf{H}(\mathbf{q})]\delta\mathbf{y}$ for (47) and V satisfies

$$
\lambda_{\min}([\mathbf{H}(\mathbf{q})])\,\|\delta\mathbf{y}\|^2 \le V \le \lambda_{\max}([\mathbf{H}(\mathbf{q})])\,\|\delta\mathbf{y}\|^2 \tag{48}
$$

Differentiating V with respect to time yields

$$
\begin{aligned}
\dot{V} &= -2\delta\mathbf{y}^T\begin{bmatrix}[\mathbf{L}] + \frac{[\mathbf{c}]_i + [\mathbf{c}]_i}{2} & \mathbf{0} & \mathbf{0}\\ \mathbf{0} & [\mathbf{S_c}]_o & \mathbf{0}\\ \mathbf{0} & \mathbf{0} & [\mathbf{S}_{\tilde{\mathbf{b}}}]_o\end{bmatrix}\delta\mathbf{y} + 2\delta\mathbf{y}_2{}^T\delta\{\mathrm{P}_{\mathbf{c}}(\mathbf{c}, \mathbf{y}_2)\}_o\\
&\quad + 2\delta\mathbf{y}_3{}^T\delta\{\mathrm{P}_{\mathbf{b}}(\hat{\mathbf{b}}, \mathbf{y}_3 + \mathbf{b})\}_o - 2\delta\mathbf{y}_3{}^T[\mathbf{S}_{\hat{\mathbf{b}}}]_o\{\mathbf{b}_r\}_o\\
&\le -2\delta\mathbf{y}^T\begin{bmatrix}[\mathbf{L}] + \frac{[\mathbf{c}]_i + [\mathbf{c}]_i}{2} & \mathbf{0} & \mathbf{0}\\ \mathbf{0} & [\mathbf{S_c}]_o & \mathbf{0}\\ \mathbf{0} & \mathbf{0} & [\mathbf{S}_{\tilde{\mathbf{b}}}]_o\end{bmatrix}\delta\mathbf{y}
\end{aligned}
\tag{49}
$$

where we used the skew-symmetric property of $[\dot{\mathcal{M}}'] - 2[\mathcal{C}'] = ([\dot{\mathcal{M}}']_{\text{other}} - 2[\mathcal{C}']_{\text{other}}) \oplus ([\dot{\mathcal{M}}']_{\text{tr}} - 2[\mathcal{C}']_{\text{tr}})$, based on the assumption in (1). Also, the inequality holds due to the definitions in (36), involving projection operators as well as $\{\tilde{\mathbf{b}}\}_o^T(\{\mathbf{b}\} + [\text{sgn}(\{\hat{\mathbf{b}}\})]\{\mathbf{b}_{\max}\})_o > 0$.

Hence, the virtual $\mathbf{y}$-system (47) is contracting *iff* $[\mathbf{L}] + ([\mathbf{c}]_i + [\mathbf{c}]_i^T)/2 = k_0\mathbf{I}_{(n-3)p} \oplus \big([\mathbf{L}]_{\text{tr}} + ([\mathbf{c}]_{\text{tr},i} + [\mathbf{c}]_{\text{tr},i}^T)/2\big) > 0$. In general, the adaptive Laplacian matrix $[\mathbf{c}]_{\text{tr}}$ is indefinite, and might have eigenvalues with both signs. Recalling Weyl's theorem[11] of $\lambda_{\min}(\mathbf{A}) + \lambda_{\min}(\mathbf{B}) \le \lambda_{\min}(\mathbf{A} + \mathbf{B})$, we can obtain

$$
\lambda_{\min}\left([\mathbf{L}]_{\text{tr}} + ([\mathbf{c}]_{\text{tr},i} + [\mathbf{c}]_{\text{tr},i}^T)/2\right) \ge k_0\mathbf{I}_{3p}, \quad \exists k_0 > 0 \tag{50}
$$

if $k_1(t) - 2k_2(t) = k_0 - \lambda_{\min}\left(([\mathbf{c}(t)]_{\text{tr},i} + [\mathbf{c}(t)]_{\text{tr},i}^T)/2\right) > 0$ where the subscript i indicates the matrix of $[\mathbf{c}]_{\text{tr}}$ whose entries are within the boundary, and we used $\lambda_{\min}([\mathbf{L}]_{\text{tr}}) = k_1 - 2k_2$.
As a result, it follows from (44) and (48-50)

$$
\dot{V} \le -2k_0\,\|\delta\mathbf{y}\|^2 \le -2\frac{k_0}{\lambda_{\max}(\mathbf{H}(\mathbf{q}))}V \tag{51}
$$

which indicates that the virtual $\mathbf{y}$ system is contracting (i.e., all of its solutions converge to each other) by Lemma 3. Without the RHS of (47) (i.e., no disturbance terms), this would imply that $\mathbf{u}'$ exponentially tends to $\mathbf{0}$ from any initial conditions. In the presence of disturbances, we need to quantify the size of the error ball.

Following Lemma 4, we define the distance between trajectories of (47) and its unperturbed dynamics as $R_1(t) = \int_{P_1}^{P_2} \|\delta\mathbf{z}\| = \int_{P_1}^{P_2} \|\boldsymbol{\Theta}\delta\mathbf{y}\|$ with $\boldsymbol{\Theta}^T\boldsymbol{\Theta} = \mathbf{H}(\mathbf{q})$. Computing the time-derivative of $R_1(t)$ results in

$$\dot{R}_1(t) + \frac{k_0}{\lambda_{\max}(\mathbf{H}(\mathbf{q}))} R_1(t) \leq \|\boldsymbol{\Theta}^{-T}\| \|\{\boldsymbol{\Delta}'_{\text{dist}}\} + [\mathcal{Y}]_i\{\tilde{\mathbf{b}}\}_i\|$$

After exponential transients ($t \to \infty$), the path integral between $\mathbf{y}_1 = \mathbf{u}'(t)$ and $\mathbf{y}_1 = \mathbf{0}$ can be defined as

$$\int_{\mathbf{0}}^{\mathbf{u}'} \|\delta\mathbf{y}_1\| \leq \frac{\lambda_{\max}(\mathbf{H}(\mathbf{q}))}{k_0 \lambda_{\min}(\mathbf{H}(\mathbf{q}))} \left(\|\{\boldsymbol{\Delta}_{\text{dist}}\}\| + \|[\mathcal{Y}]\{\tilde{\mathbf{b}}\}\| \right)$$

since the modeling error $\|[\mathcal{Y}]_i\{\tilde{\mathbf{b}}\}_i\| \leq \|[\mathcal{Y}]\{\tilde{\mathbf{b}}\}\|$ and $\|\delta\mathbf{y}_1\| \leq \|\delta\mathbf{y}\|$.

Based on (19), we can define the virtual system of $\mathbf{y}_4$ hierarchically combined with the system of $\mathbf{y}$ in (47):

$$\dot{\mathbf{y}}_4 + \lambda''\mathbf{I}_{np}\mathbf{y}_4 - \{\dot{\mathbf{q}}'_d(t)\} - \lambda''\mathbf{I}_{np}\{\mathbf{q}'_d(t)\} = \mathbf{y}_1 \tag{52}$$

where $\{\mathbf{q}'_d(t)\}$ is obtained by stacking the common $\mathbf{q}'_d(t)$ p times. This has a particular solution of $\mathbf{y}_4 = \{(\mathbf{T}^T\mathbf{q}'')'\}$ and $\mathbf{y}_1 = \mathbf{u}'$ where $\{(\mathbf{T}^T\mathbf{q}'')'\}$ denotes a concatenated vector of the first n-elements of each $\mathbf{T}_{j-1}^T\mathbf{q}''_j \in \mathbb{R}^{n+1}$. Another solution is $\mathbf{y}_4 = \{\mathbf{q}'_d(t)\}$ with $\mathbf{y}_1 = \mathbf{0}$.

Consequently, the path integral $R_2(t)$ from (43) verifies

$$\dot{R}_2(t) + \lambda'' R_2(t) \leq \sup_t \int_{\mathbf{0}}^{\mathbf{u}'} \|\delta\mathbf{y}_1\| \tag{53}$$

Hence, by applying Lemmas 4 and 5, we can find that the error converges to a ball defined by (43) as $t \to \infty$. ■

Corollary 7 One drawback of (44) is that computing $\lambda_{\min}\left([\mathbf{c}(t)]_{\text{tr},i} + [\mathbf{c}(t)]_{\text{tr},i}^T\right)$ in realtime can be computationally expensive for a very large network (i.e., large p) unless the idea of fragmentation is used (see Sect D). A more conservative bound of $[\mathbf{c}]_{\text{tr}}$ can be used to compute the fixed gains k_1 and k_2. A trade-off is that this leads to a larger gain for a large p than (44).

$$k_1 - 2k_2 = k_0 + \min\left(\begin{matrix} \sqrt{((p-1)\varrho_m + \varrho_0)(m_n\varrho_m + \varrho_0)}c_{\max} \\ (m_n\varrho_m + \varrho_0)c_{\max} \end{matrix} \right) \tag{54}$$

where we assume that the maximum values of the distance-based connectivity function $\varrho_{jk}(d_{jk}) < 1$ are known a priori as $\varrho_0 = \sup_j \varrho_{jj}(0)$ (for the self-gain) and ϱ_m (for neighbors, $j \neq k$). Also, we used $\|[\mathbf{c}]_{\text{tr},i}\| \leq \|[\mathbf{c}]_{\text{tr}}\|$, $\|[\mathbf{c}]_{\text{tr}}\|_1 \leq ((p-1)\varrho_m + \varrho_0)c_{\max}$, $\|[\mathbf{c}]_{\text{tr}}\|_\infty \leq (m_n\varrho_m + \varrho_0)c_{\max}$, and $\|[\mathbf{c}]_{\text{tr}}\| = \sqrt{\|[\mathbf{c}]_{\text{tr}}\|_\infty \|[\mathbf{c}]_{\text{tr}}\|_1}$ while m_n is the maximum number of neighbors for $[\mathbf{c}]_{\text{tr}}$. Also, the spectral density $\rho([\mathbf{c}]_{\text{tr}}) \leq \|[\mathbf{c}]_{\text{tr}}\|$ for any norm is used. If ϱ_m is not known, we can use $\varrho_m < \varrho_0 < 1$.

Remark 8 The phase synchronization law in (22) suggests a flexible control design for a complex networked EL system since a control designer need not fix the coupling gains and network topologies a priori. This is useful when robots go through numerous reconfigurations.

C. Tighter Error Bounds for Synchronization

We show herein that the control law (22) guarantees both faster and tighter synchronization of the coupled variables than tracking. Since $\mathbf{u}'_{\text{other}}$ are not coupled (see Remark 7), we consider only the translational motions in this section (i.e., $\mathbf{q}_j \in \mathbb{R}^3$ and $\mathbf{u}' = \mathbf{u}'_{\text{tr}}$).

Definition 2 Synchronization flow-invariant manifold. *According to (19), each transformed composite variable $\mathbf{u}'_j$ is expressed with respect to the common leader trajectory $\mathbf{q}'_d(t)$. Since the difference between $\mathbf{u}'_j$ and $\mathbf{u}'_k$ cancels this common $\mathbf{q}'_d(t)$ (20), the synchronization manifold is defined as $\mathbf{V}_{\text{sync}}^T\mathbf{u}'_{\text{tr}} = \mathbf{0}$ where the matrix $\mathbf{V}_{\text{sync}} \in \mathbb{R}^{3p\times 3(p-1)}$ is an orthonormal matrix of eigenvalues of $[\mathbf{L}]_{\text{tr}}$ other than $[\mathbf{1}] = \frac{1}{\sqrt{p}}[\mathbf{I}_3, \mathbf{I}_3, \cdots, \mathbf{I}_3]^T \in \mathbb{R}^{3p\times 3}$ (i.e., $\mathbf{V}_{\text{tr}} = \left[[\mathbf{1}],\ \mathbf{V}_{\text{sync}}\right]$, $\mathbf{V}_{\text{tr}}\mathbf{V}_{\text{tr}}^T = \mathbf{V}_{\text{tr}}^T\mathbf{V}_{\text{tr}} = \mathbf{I}_{3p}$). Since $[\mathbf{L}]_{\text{tr}}$ represents a regular graph, $[\mathbf{1}]$ should be its eigenvectors. By spectral decomposition,[3] $\mathbf{V}_{\text{tr}}^T[\mathbf{L}]_{\text{tr}}\mathbf{V}_{\text{tr}}$ verifies*

$$= \begin{bmatrix} [\mathbf{1}]^T[\mathbf{L}]_{\text{tr}}[\mathbf{1}] & [\mathbf{1}]^T[\mathbf{L}]_{\text{tr}}\mathbf{V}_{\text{sync}} \\ \mathbf{V}_{\text{sync}}^T[\mathbf{L}]_{\text{tr}}[\mathbf{1}] & \mathbf{V}_{\text{sync}}^T[\mathbf{L}]_{\text{tr}}\mathbf{V}_{\text{sync}} \end{bmatrix} = \begin{bmatrix} (k_1-2k_2)\mathbf{I}_3 & \mathbf{0} \\ \mathbf{0} & \mathbf{D}_s \end{bmatrix} \tag{55}$$

where the block diagonal matrix $\mathbf{D}_s = \mathbf{V}_{\text{sync}}^T[\mathbf{L}]_{\text{tr}}\mathbf{V}_{\text{sync}}$ verifies $\lambda_{\min}(\mathbf{D}_s) > k_1 - 2k_2$.

By pre-multiplying (46) by $\mathbf{V}_{\rm tr}^T$, we can obtain

$$\mathbf{V}_{\rm tr}^T[\mathcal{M}']\mathbf{V}_{\rm tr}\dot{\mathbf{y}}_{\mathbf{v}} + \mathbf{V}_{\rm tr}^T\left([\mathcal{C}'] + [\mathbf{L}] + [\mathbf{c}]_{\rm sym}\right)\mathbf{V}_{\rm tr}\mathbf{y}_{\mathbf{v}} = \mathbf{V}_{\rm tr}^T\mathbf{d}(t)$$

where $\mathbf{d}(t) = \{\mathbf{\Delta}'_{\rm dist}\} + [\mathcal{Y}]\{\tilde{\mathbf{b}}\}$ and $[\mathbf{c}]_{\rm sym} = ([\mathbf{c}] + [\mathbf{c}]^T)/2$. This system has $\mathbf{y}_{\mathbf{v}} = \mathbf{V}_{\rm tr}^T\mathbf{u}'_{\rm tr}$ as its particular solution. Furthermore, $\mathbf{y}_{\mathbf{v}} = \mathbf{V}_{\rm tr}^T\mathbf{u}'_{\rm tr}$ can be decomposed into tracking and synchronization errors:

$$\mathbf{y}_{\mathbf{v}} = \begin{bmatrix} \mathbf{y}_t \\ \mathbf{y}_s \end{bmatrix} = \begin{bmatrix} [\mathbf{1}]^T\mathbf{u}'_{\rm tr} \\ \mathbf{V}_{\rm sync}^T\mathbf{u}'_{\rm tr} \end{bmatrix} \tag{56}$$

Theorem 8 *Synchronization occurs faster than tracking control, and the synchronization error is smaller than the tracking control error if* $\|[\mathbf{1}]^T\mathbf{d}(t)\| > \|\mathbf{V}_{\rm sync}^T\mathbf{d}(t)\|$.

Proof: Similar to (49), we define the modified virtual length $V_{\mathbf{v}} = \delta\mathbf{y}_{\mathbf{v}}^T\left(\mathbf{V}_{\rm tr}^T[\mathcal{M}']\mathbf{V}_{\rm tr}\right)\delta\mathbf{y}_{\mathbf{v}}$

$$\dot{V}_{\mathbf{v}} \le -2\delta\mathbf{y}_{\mathbf{v}}^T\mathbf{V}_{\rm tr}^T\left([\mathbf{L}] + [\mathbf{c}]_{\rm sym}\right)\mathbf{V}_{\rm tr}\delta\mathbf{y}_{\mathbf{v}} \tag{57}$$

From (55), $\mathbf{V}_{\rm tr}^T([\mathbf{L}] + [\mathbf{c}]_{\rm sym})\mathbf{V}_{\rm tr} > 0$ is equivalent to

$$\begin{aligned} &\begin{bmatrix} (k_1-2k_2)\mathbf{I}_3 & \mathbf{0} \\ \mathbf{0} & \mathbf{D}_s \end{bmatrix} + [\mathbf{c}]_{\rm sym} \\ &\ge \begin{bmatrix} (k_1-2k_2)\mathbf{I}_3+\lambda_{\min}([\mathbf{c}]_{\rm sym})\mathbf{I}_3 & \mathbf{0} \\ \mathbf{0} & \mathbf{D}_s+\lambda_{\min}([\mathbf{c}]_{\rm sym})\mathbf{I}_{3(p-1)} \end{bmatrix} > 0 \end{aligned} \tag{58}$$

The gains k_1 and k_2 can be chosen to ensure that the contraction rate for synchronization (λ_s) is larger than that of tracking control (λ_t)

$$\lambda_s = \frac{\mathbf{D}_s + \lambda_{\min}([\mathbf{c}]_{\rm sym})}{\lambda_{\max}([\mathbf{1}]^T[\mathcal{M}'][\mathbf{1}])} > \lambda_t = \frac{k_1 - 2k_2 + \lambda_{\min}([\mathbf{c}]_{\rm sym})}{\lambda_{\max}(\mathbf{V}_{\rm sync}^T[\mathcal{M}']\mathbf{V}_{\rm sync})}$$

since $\lambda_{\min}(\mathbf{D}_s) > k_1 - 2k_2$. Furthermore, if $\|[\mathbf{1}]^T\mathbf{d}(t)\| > \|\mathbf{V}_{\rm sync}^T\mathbf{d}(t)\|$ (i.e., the disturbance flow field is more codirectional), the synchronization error is smaller than the tracking error since $\|[\mathbf{1}]^T\mathbf{d}(t)\|/\lambda_t > \|\mathbf{V}_{\rm sync}^T\mathbf{d}(t)\|/\lambda_s$ and assuming the cross-coupling terms, $\|[\mathbf{1}]^T[\mathcal{M}']\mathbf{V}_{\rm sync}\|$ and $\|[\mathbf{1}]^T[\mathcal{C}']\mathbf{V}_{\rm sync}\|$ are sufficiently small. ■

D. Hierarchical Decomposition for Multiple Ellipses

For Theorem 6, we assumed that agents are located in the same elliptical orbit. The formation control and phase synchronization controller in (22) can be modified for phase synchronization in multiple ellipses if the ellipses share the same relative orbital plane.

Corollary 9 *If the p agents follow multiple concentric ellipses in the same plane, Theorems 6 and 8 hold with*

$$\begin{aligned} &\begin{bmatrix} \mathbf{R}_{\rm f}\boldsymbol{\tau}_j(t) \\ \tau_{jZ'} \end{bmatrix} = \begin{bmatrix} \mathbf{Y}_j(\mathbf{q}'_j,\dot{\mathbf{q}}'_j,\dot{\mathbf{q}}'_{j,r},\ddot{\mathbf{q}}'_{j,r})\hat{\mathbf{b}}_j \\ Y_{jZ'}\hat{\mathbf{b}}_j \end{bmatrix} + \begin{bmatrix} \mathbf{R}_{\rm f}\mathbf{G}_j(\mathbf{R}_{\rm f}^T\mathbf{q}'_j) \\ G_{jZ'} \end{bmatrix} \\ &+ \begin{bmatrix} -k_0\mathbf{s}''_{j,\rm other} \\ -k_1(t)\mathbf{s}''_{j,\mathbf{tr}} + k_2(t)\frac{2}{m_o}\sum_{i\in\mathcal{N}_j(t)}^{m_o}\mathbf{\Upsilon}_{j-i}\mathbf{s}''_{i,\rm tr} \end{bmatrix} - \begin{bmatrix} \mathbf{0}_{(n-3)\times 1} \\ \mathbf{W}_j(\mathbf{\Upsilon}\mathbf{s}''_{\rm tr},\boldsymbol{\varrho}_j)\mathbf{c}_j \end{bmatrix} \end{aligned}$$

where $\mathbf{s}''_{i,\rm tr}$ *denotes the composite variable of the translational motion for the* i*th agent, defined in (17) and*

$$\begin{aligned} \mathbf{\Upsilon}_{j-i} &= \frac{l_{\min,j}}{l_{\min,1}}\mathbf{T}'((j-1)\phi_j)\left(\frac{l_{\min,i}}{l_{\min,1}}\mathbf{T}'((i-1)\phi_i)\right)^{-1} \\ &= \frac{l_{\min,j}}{l_{\min,i}}\mathbf{T}'((j-1)\phi_j - (i-1)\phi_i) \\ \mathbf{\Upsilon}\mathbf{s}''_{\rm tr} &= \left[\mathbf{\Upsilon}_{j-1}\mathbf{s}''_{1,\rm tr},\ \mathbf{\Upsilon}_{j-2}\mathbf{s}''_{2,\rm tr},\ \cdots,\ \mathbf{\Upsilon}_{j-p}\mathbf{s}''_{p,\rm tr}\right] \end{aligned} \tag{59}$$

where ϕ_j *is the phase angle difference of the* j*th agent in its ellipse, and* $l_{\min,j}$ *is the radius of the elliptical orbit where the* j*th agent is located.*

Proof: The proof follows the proof of Theorem 6 by replacing $\mathbf{T}'_{j-l}$ and $\mathbf{T}'^{T}_{j-l}$ by $\boldsymbol{\Upsilon}_{j-l}$ and $\boldsymbol{\Upsilon}^{-1}_{j-l}$. ■

Remark 9 *Concurrent Synchronization by Hierarchical Connections.* If the number of robots ($= p$) in the network increases, the computational burden of computing $k_1(t)$ and $k_2(2)$ increases (44) or we need larger gains from (54). One method of avoiding the curse of dimensionality is to use fragmentation, i.e., the network is divided into subgroups. We can achieve the concurrent synchronization[3] of multiple subgroups by picking a leader trajectory input ($\mathbf{q}_d(t)$) from a different orbit or ellipse. Such an exploitation of mixing two different types of inputs (leader-follower and diffusive couplings) results in hierarchical decomposition of a complex network. In this case, $\mathbf{c}_j$ can be limited to only members in the subgroup, so that the structure of the adaptive system can be simpler in terms of the computation and communication burdens. Corollary 9 can be used to define phase synchronization between different elliptical orbits.

VI. Numerical Simulation and Discussion

We show the effectiveness of the proposed synchronization controller by investigating a challenging scenario of reconfiguring 50 spacecraft (S/C) from uniformly distributed initial conditions ($[-0.25, 0.25]$ km) to four different elliptical orbits. We assume that 5, 10, 15, 20 S/C are placed from the 1st to the 4th target relative orbits, where the size between the first and ith ellipses ($i = 2, 3, 4$) is i.

We use (3) in Example 1 for the relative motion of each spacecraft with respect to the chief (mean) orbital motion. We choose $m_j = 100$ kg, $A_j = 1$ m^2, $C_D = 2.0$, and $[a_0,\ e_0,\ i_0,\ \Omega_0,\ \omega_0,\ \nu_0] = [R_E + 400,\ 0,\ 45^\circ,\ 30^\circ,\ 0^\circ,\ 10^\circ]$, where R_E denotes the radius of the Earth. $\|\boldsymbol{\Delta}_{\text{dist}}\|\text{max}/m_j = 10^{-5}$ km/s^2.

The virtual leader trajectory ($\mathbf{q}_d(t)$) in 1st orbit is determined by $x_{d,0} = 0.5$ km, $y_{d,0} = 0.5$ km, $z_{d,0} = 0.25$ km, $\dot{z}_{d,0} = 10^{-3}$ km/s and (5). Then, we can obtain the the new frame for phase synchronization as follows: $a_e = 0.5590$ km, $z_{\max} = 0.2539$ km, $\psi_{e_0} = -63.43^\circ$, $\psi_{z_0} = 79.98^\circ$, $l_{\min} = 0.6094$ km, $l_{\max} = 1.1205$ km. We can compute $\psi_x = 89.62^\circ$ and $\mathbf{R}'_{\text{f}} = \begin{bmatrix} 0.9171 & -0.0365 & 0.3969 \\ -0.3290 & 0.4929 & 0.8055 \\ -0.2250 & -0.8693 & 0.4400 \end{bmatrix}$. For the controller in (22), $k_1 = 3$, $k_2 = 1$, $\lambda'' = 0.1$, $\boldsymbol{\Sigma}_j = 10\mathbf{I}$, $c_{\max,j,k} = 1$, $\mathbf{c}_j(0) = \mathbf{0}$, $r_{\text{col},j} = 50$ m, $k_{\mathbf{Q}} = 1$, and $\dot{\mathbf{q}}_{\text{p,tr}} = 1/\sqrt{3}[1\ 1\ 1]^T$. For the communication, no more than 4 connections with neighbors are allowed ($m_n = 4$) and the parameter adaptation law in (28) is turned off.

Figure 4 shows the closed-loop trajectories of 50 S/C in 3D during the first 1000 s. Note that after

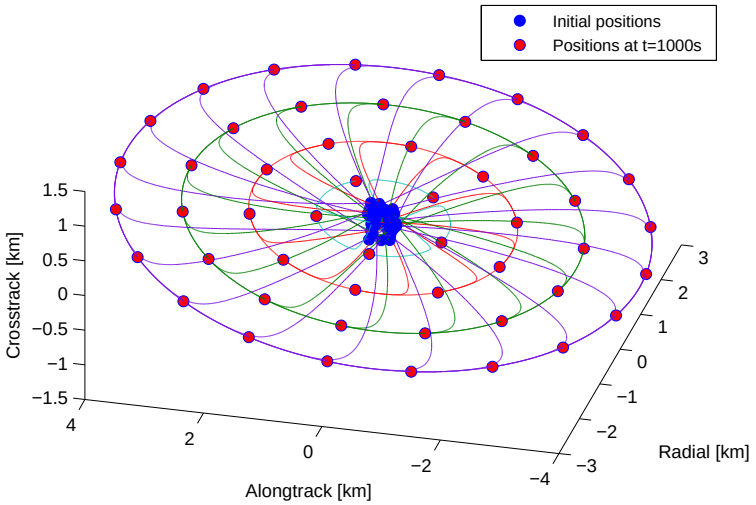

Figure 4. Trajectories of the 50 S/C for 1000 s.

reaching their target relative orbits, S/C follow their desired trajectories without a drift. The upper figure in Fig. 5 shows that the x'_j trajectories of the 50 spacecraft synchronize to the virtual leader trajectory, where x'_j is obtained by the scaling and phase shift operations of $\boldsymbol{\Upsilon}_{1-j}$ in (59).

The bottom figure in Fig. 5 shows the adaptive gain variations for the 25th S/C, which is located in the

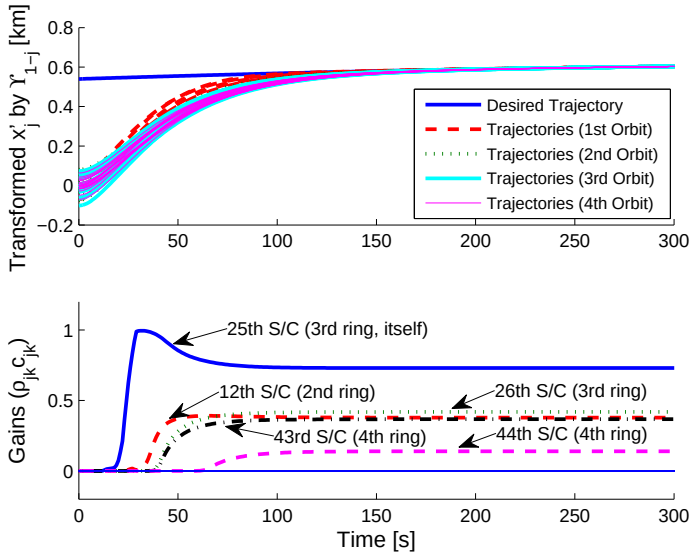

Figure 5. Trajectories of the first elements of $\Upsilon_{1-j}\mathbf{q}_j''$ $(j = 1, \cdots, 50)$ where the subscript 1 denotes the orbit leader spacecraft (upper) and the adapted diffusive gains for the 25th S/C (bottom). The time span is not long enough to show a periodic motion of x_d' from (5) with a period 5536 s.

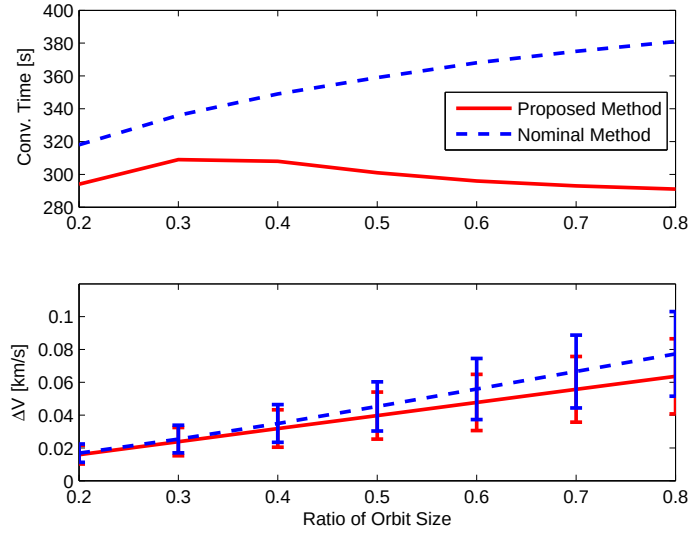

Figure 6. Comparison of the performance: the longest convergence time among all S/C with the same fuel consumption (upper figure) and average fuel consumption with the same convergence time (bottom figure)

3rd ring. The adaptive gains do not have values during 15 sec due to the zero initial conditions. Note that the 25th S/C has gains only for four of its neighbors: the 12th S/C (2nd ring),the 26th S/C (3rd ring), the 43rd and 44th S/C (4th ring).

In order to evaluate the performance, we compare the proposed synchronization controller and the nominal gain-based controller with properly tuned gains. We assume that all S/C are initially located at the origin. The first figure in Fig. 6 shows the convergence time , defined as the longest time among all S/C for $\|\mathbf{q}_{j,\mathrm{tr}} - \mathbf{q}_{d,j,\mathrm{tr}}\| \leq 1$ m $\forall j = 1, 2, \cdots, 50$, with respect to the size of the orbits (the number denotes the ratio to the orbit defined previously in this section.) with the same amount of fuel for reconfigurations. As the orbit size gets bigger, the proposed synchronization controller makes the S/C converge faster due to the gain adaptation law. On the other hand, based on the same convergence time, the proposed synchronization controller with the adaptive graph Laplacian uses less fuel (ΔV) for the reconfiguration than the nominal fixed gain controller (the bottom figure in Fig. 6). This result can be interpreted in terms of the adaptive gain profile that is varied as a function of ($\mathbf{u}'$), as shown in Fig. 5. Through these results of simulation, we showed that the proposed phase synchronization controller more efficiently synchronized the motions of the spacecraft during the reconfigurations of the swarm.

VII. Conclusions

We presented a new formation control and phase synchronization strategy for robotic networks comprised of EL systems moving in elliptical orbits. The proposed coordinate transformation and phase angle shift method facilitates phase angle rotations in arbitrary ellipses, which is essential to the phase synchronization control law. The nonlinear stability proofs of the closed-loop system were constructed by applying robust contraction analysis to virtual systems that resemble nonlinear observers, thereby establishing a connection to incremental stability. The error bound of the proposed synchronization control law is shown to be smaller than that of an uncoupled control law. This justifies the use of a synchronization framework when the synchronization error should be kept smaller than a tracking error (e.g., stellar interferometers). Another contribution of the paper lies in the adaptive scheme of automatically computing evolving network topologies, thereby eliminating the need for defining a "fixed" communication or relative sensing topology for synchronization stability. This result is useful especially when we deal with a large number of agents in robotic networks that perform arbitrary reconfiguration maneuvers. While the main motivation of this work stemmed from controlling a large number of rigid bodies in space, the proposed adaptive graph Laplacian framework is applicable to coupled dynamical systems comprised of arbitrary EL systems whether or not they move in elliptical orbits.

Acknowledgements

The research was carried out in part at the Jet Propulsion Laboratory, California Institute of Technology, under a contract with the National Aeronautics and Space Administration. ©2011 California Institute of Technology. Government sponsorship acknowledged. The authors gratefully acknowledge Lars Blackmore and Daniel Morgan for constructive comments.

References

[1]I. Chang, S.-J. Chung, and L. Blackmore. Cooperative Control with Adaptive Graph Laplacians for Spacecraft Formation Flying. In *49th IEEE Conf. Decision Control*, pages 4926–4933, Atlanta, GA, December 2010.

[2]S.-J. Chung, U. Ahsun, and J.-J. E. Slotine. Application of Synchronization to Formation Flying Spacecraft: Lagrangian Approach. *J. Guid. Control Dyn.*, 32(2):512–526, 2009.

[3]S.-J. Chung and J.-J. E. Slotine. Cooperative Robot Control and Concurrent Synchronization of Lagrangian Systems. *IEEE Trans. Robot.*, 25(3):686–700, 2009.

[4]J. Cortés, S. Martínez, T. Karataş, and F. Bullo. Coverage Control for Mobile Sensing Networks. *IEEE Trans. Robot. Autom.*, 20(2):243–255, 2004.

[5]F. Cucker and S. Smale. Emergent Behavior in Flocks. *IEEE Trans. Autom. Control*, 52(5):852–862, 2007.

[6]J. A. Fax and R. M. Murray. Information Flow and Cooperative Control of Vehicle Formations. *IEEE Trans. Autom. Control*, 49(9):1465–1476, 2004.

[7]T. Glotzbach, M. Schneider, M. Jacobi, and P. Otto. Obstacle Avoidance for Multiple Unmanned Marine Vehicles (MUMVs) in Close Formation. In *OCEANS 2009*, pages 1–10, Bremen, Germany, May 2009.

[8]F. Y. Hadaegh, S.-J. Chung, and H. Manaroha. Development and Flight of Swarms of 100-gram Satellites. *IEEE Syst.*

J., 2011. (to be submitted).

[9]Y. Hong, G. Chen, and L. Bushnell. Distributed Observers Design for Leader-Following Control of Multi-Agent Networks. *Automatica*, 44(3):846–850, 2006.

[10]Y. Hong, J. Hu, and L. Gao. Tracking Control for Multi-Agent Consensus with an Active Leader and Variable Topology. *Automatica*, 42(7):1177–1182, 2006.

[11]R. A. Horn and C. R. Johnson. *Matrix Analysis*. Cambridger University Press, New York, NY, 1985.

[12]I.-A. F. Ihle, M. Arcak, and T. I. Fossen. Passivity-Based Designs for Synchronized Path-Following. *Automatica*, 43(9):1508–1518, 2007.

[13]H. K. Khalil. *Nonlinear Systems, 3rd edition*. Prentice Hall, Upper Saddle River, NJ, 2001.

[14]T.-H. Kim and T. Sugie. Cooperative Control for Target-Capturing Task Based on a Cyclic Pursuit Strategy. *Automatica*, 43(8):1426–1431, 2007.

[15]M. Krstić, I. Kanellakopoulos, and P. Kokotović. *Nonlinear and Adaptive Control Design*. John Wiley & Sons, Inc., New York, NY, 1995.

[16]W. Lohmiller and J.-J. E. Slotine. On Contraction Analysis for Non-Linear Systems. *Automatica*, 34(6):683–696, 1998.

[17]D. Morgan, S.-J. Chung, L. Blackmore, B. Açıkmeşe, D. Bayard, and F. Y. Hadaegh. Swarm Keeping Strategies for Spacecraft under J_2 and Atmospheric Drag Perturbations. *Journal of Guidance, Control, and Dynamics*, 2011. under review. available at `http://netfiles.uiuc.edu/sjchung/www/publications.html`.

[18]D. Nešić and A. R. Teel. Input-to-State Stability of Networked Control Systems. *Automatica*, 40(12):2121–2128, 2004.

[19]R. Olfati-Saber and R. M. Murray. Consensus Problems in Networks of Agents with Switching Topology and Time-Delays. *IEEE Trans. Autom. Control*, 49(9):1520–1533, 2004.

[20]S. Park, J. Deyst, and J. P. How. Performance and Lyapunov Stability of a Nonlinear Path-Following Guidance Method. *J. Guid. Control Dyn.*, 30(6):1718–1728, 2007.

[21]Q. C. Pham and J.-J. E. Slotine. Stable Concurrent Synchronization in Dynamic System Networks. *Neural Networks*, 20(1):62–77, 2007.

[22]J.-B. Pomet and L. Praly. Adaptive Nonlinear Regulation: Estimation from the Lyapunov Equation. *IEEE Trans. Autom. Control*, 37(6):729–740, 1992.

[23]W. Ren. Distributed Leaderless Consensus Algorithms for Networked Euler-Lagrange Systems. *Int. J. Control*, 82(11):2137–2149, 2009.

[24]W. Ren and R. W. Beard. Consensus Seeking in Multiagent Systems Under Dynamically Changing Interaction Topologies. *IEEE Trans. Autom. Control*, 50(5):655–661, 2005.

[25]B. S. Rüffer, C. M. Kellett, and S. R. Weller. Connection Between Cooperative Positive Systems and Integral Input-to-State Stability of Large-Scale Systems. *Automatica*, 46(6):1019–1027, 2010.

[26]D. P. Scharf, F. Y. Hadaegh, and S. R. Ploen. A Survey of Spacecraft Formation Flying Guidance and Control (Part I): Guidance. In *Amer. Control Conf.*, pages 1733–1739, Denver, CO, June 2003.

[27]J.-J. E. Slotine and W. Li. *Applied Nonlinear Control*. Prentice Hall, Englewood Cliffs, NJ, 1991.

[28]R. S. Smith and F. Y. Hadaegh. Closed-Loop Dynamics of Cooperative Vehicle Formations with Parallel Estimators and Communication. *IEEE Trans. Autom. Control*, 52(8):1404–1414, 2007.

[29]D. J. Stilwell and B. E. Bishop. Platoons of Underwater Vehicles. *IEEE Control Syst. Mag.*, 20(6):45–52, 2000.

[30]M. V. Subbotin and R. S. Smith. Design of Distributed Decentralized Estimators for Formations with Fixed and Stochastic Communication Topologies. *Automatica*, 45(11):2491–2501, 2009.

[31]W. Wang and J.-J. E. Slotine. A Theoretical Study of Different Leader Roles in Networks. *IEEE Trans. Autom. Control*, 51(7):1156–1161, 2006.